Ion Adsorption at the Rutile−Water Interface: Linking Molecular and Macroscopic Properties

Z. Zhang,[†,‡] P. Fenter,*[,†] L. Cheng,[†] N. C. Sturchio,[†,§] M. J. Bedzyk,[†,‡] M. Předota,[∥,⊥] A. Bandura,[○] J. D. Kubicki,[#] S. N. Lvov,[#] P. T. Cummings,[⊥] A. A. Chialvo,[▽] M. K. Ridley,[◆] P. Bénézeth,[▽] L. Anovitz,[▽] D. A. Palmer,[▽] M. L. Machesky,[+] and D. J. Wesolowski[▽]

Argonne National Laboratory, ER-203, Argonne, Illinois 60439, Northwestern University, Institute of Environmental Catalysis, Evanston, Illinois 60208, University of Illinois at Chicago, Chicago, Illinois 60607, Institute of Chemical Process Fundamentals, 16502 Prague, Czech Republic, Vanderbilt University, Nashville, Tennessee 37235, St. Petersburg State University, St. Petersburg, Russia, The Pennsylvania State University, University Park, Pennsylvania 16802, Oak Ridge National Laboratory, Oak Ridge, Tennessee 37831, Texas Tech University, Lubbock, Texas 79409, and Illinois State Water Survey, Champaign, Illinois 61820

Received July 29, 2003. In Final Form: March 10, 2004

A comprehensive picture of the interface between aqueous solutions and the (110) surface of rutile (α-TiO_2) is being developed by combining molecular-scale and macroscopic approaches, including experimental measurements, quantum calculations, molecular simulations, and Gouy−Chapman−Stern models. In situ X-ray reflectivity and X-ray standing-wave measurements are used to define the atomic arrangement of adsorbed ions, the coordination of interfacial water molecules, and substrate surface termination and structure. Ab initio calculations and molecular dynamics simulations, validated through direct comparison with the X-ray results, are used to predict ion distributions not measured experimentally. Potentiometric titration and ion adsorption results for rutile powders having predominant (110) surface expression provide macroscopic constraints of electrical double layer (EDL) properties (e.g., proton release) which are evaluated by comparison with a three-layer EDL model including surface oxygen proton affinities calculated using ab initio bond lengths and partial charges. These results allow a direct correlation of the three-dimensional, crystallographically controlled arrangements of various species (H_2O, Na^+, Rb^+, Ca^{2+}, Sr^{2+}, Zn^{2+}, Y^{3+}, Nd^{3+}) with macroscopic observables (H^+ release, metal uptake, zeta potential) and thermodynamic/electrostatic constraints. All cations are found to be adsorbed as "inner sphere" species bonded directly to surface oxygen atoms, while the specific binding geometries and reaction stoichiometries are dependent on ionic radius. Ternary surface complexes of sorbed cations with electrolyte anions are not observed. Finally, surface oxygen proton affinities computed using the MUSIC model are improved by incorporation of ab initio bond lengths and hydrogen bonding information derived from MD simulations. This multitechnique and multiscale approach demonstrates the compatibility of bond-valence models of surface oxygen proton affinities and Stern-based models of the EDL structure, with the actual molecular interfacial distributions observed experimentally, revealing new insight into EDL properties including specific binding sites and hydration states of sorbed ions, interfacial solvent properties (structure, diffusivity, dielectric constant), surface protonation and hydrolysis, and the effect of solution ionic strength.

1. Introduction

A pervasive characteristic of the metal oxide−water interface is the spontaneous and pH-dependent charge development that results from the preferential adsorption or desorption of ions in the interfacial region.[1,2] This charging behavior is usually quantified by applying various surface complexation models (SCMs), in which mass law expressions describing ion binding by reactive groups at the metal oxide surface are coupled with classical compact/diffuse-layer models of the electrical double layer (EDL), which correct for the change in electrical potential across the EDL upon charging.[3,4] Common to SCMs is the assumption that surface charge is principally determined by proton uptake and release by oxygen atoms at the crystal surface, with the resulting charge compensated by aqueous ions distributed among discrete ("Stern" or "Helmholtz") planes of cation and anion adsorption, as well as a diffuse layer of ions typically described by Gouy−Chapman theory. A generic 2-p*K* formalism has been used most often to describe proton affinity for surface oxygen atoms.[5,6] Surface complexation models have been successful in rationalizing macroscopic ion adsorption data, but the detailed structure (or lack of structure) of the EDL

* Corresponding author. E-mail: Fenter@anl.gov.
† Argonne National Laboratory.
‡ Northwestern University.
§ University of Illinois at Chicago.
∥ Institute of Chemical Process Fundamentals.
⊥ Vanderbilt University.
○ St. Petersburg State University.
The Pennsylvania State University.
▽ Oak Ridge National Laboratory.
◆ Texas Tech University.
+ Illinois State Water Survey.

(1) Stumm, W. *Chemistry of the Solid-Water Interface*; Wiley-Interscience: New York, 1995.
(2) Lyklema, J. *Fundamentals of Interface and Colloid Science*; Academic Press: New York, 1995; Vol. II.
(3) Dzombak, D.; Morel, F. M. M. *Surface Complexation Modeling-Hydrous Ferric Oxide*; Wiley-Interscience: New York, 1990.
(4) Hiemstra, T.; Van Riemsdijk, W. H. In *Encyclopedia of Colloid and Interface Science*; Hubbard, A. T., Ed.; Marcel Dekker: New York, 2002; pp 3773−3799.
(5) Parks, G. A.; DeBruyn, P. L. *J. Phys. Chem.* **1962**, *66*, 967−973.
(6) Schindler, P. W.; Stumm, W. In *Aquatic Surface Chemistry*; Stumm, W., Ed,; Wiley-Interscience: New York, 1987; pp 83−110.

10.1021/la0353834 CCC: $27.50
Published on Web 05/07/2004

used in these models is generally assumed and can vary considerably among SCMs. Consequently, the resulting model parameters (binding constants, Stern-layer capacitances, total site densities, reaction stoichiometries, etc.) are not unique and can be highly covariant.[7] The MUSIC model[8,9] was the first surface protonation scheme developed which utilizes the specific crystal surface structure and the bond valence concept,[10,11] together with an empirical relationship between valence undersaturation and proton affinities of oxygen ligands in bulk solutions, to explicitly predict surface oxygen proton affinities and site densities. Such models provide an opportunity for incorporation of atomic-scale experimental observations and computational predictions of the interfacial structure and properties.

Most previous studies of rutile−water interactions have been performed in ultrahigh vacuum or have involved rutile surfaces exposed to low-pressure water vapor (refs 12−14; for extensive reviews, see refs 15 and 16 and references therein). While the interaction of water with metal oxide surfaces has been studied with various experimental and theoretical approaches,[17] recent advances in understanding the structure and properties of oxide surfaces in contact with dense aqueous solutions have been made with synchrotron X-ray spectroscopic and scattering techniques including X-ray absorption spectroscopy,[18,19] surface X-ray scattering,[20] and X-ray standing waves.[21] These approaches make use of the ability of high-energy X-rays to penetrate aqueous solutions, revealing a more precise understanding of oxide−water interfacial structure at the molecular scale. Computational approaches are also being developed for predicting interfacial structures and dynamics (ref 22 and references therein). However, these advances have not been fully integrated with constraints derived from macroscopic ion adsorption results and have not been extensively employed in testing existing SCMs or developing new mathematical descriptions that are able to link atomic-scale observations and computations with the macroscopic manifestations of interfacial phenomena.

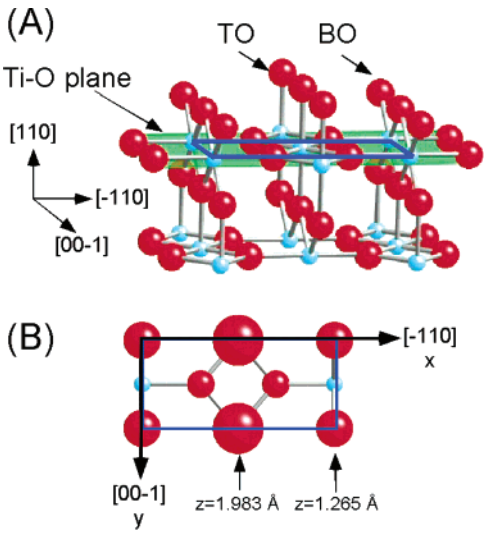

Figure 1. (A) Schematic of the rutile surface unit cell showing the surface unit cell, BO and TO rows, the crystallographic directions (in bulk Bragg notation), and the Ti−O surface plane (shaded green) which is the reference plane from which all ion heights are reported. (B) Top view of the surface unit cell indicating the nominal heights of the BO and TO sites with respect to the Ti−O surface plane.

In this study, we combine in situ synchrotron X-ray measurements on submerged rutile (110) single-crystal surfaces with ab initio calculations, molecular-dynamic simulations, and macroscopic ion adsorption data from rutile powders to obtain an integrated understanding of the solution−crystal interface that connects the actual molecular structures to the macroscopic properties. This crystallographic surface of rutile was chosen for these studies because it is highly stable and is one of the most important and extensively investigated oxide surfaces across a broad range of disciplines and applications[15,16] Our long-range goals are to establish a link between macroscopic manifestations of metal oxide surface charging and ion adsorption and the molecule-scale interfacial structures, to provide a test-bed for comparing experimental and computational methods of obtaining molecular-level information, and to facilitate incorporation of such information into improved SCMs.

The starting point of this work is the expected structure of the rutile (110) surface, as shown in Figure 1. The surface unit mesh has dimensions, $a = 6.497$ Å and $b = 2.959$ Å along the rutile [$\bar{1}$10] and [001] crystallographic directions. In this schematic, the rutile surface has a complete Ti−O layer (referred to as the "surface plane") which is overlain by two distinct rows of oxygen atoms. These two rows are doubly and singly coordinated with the titanium atoms in the surface plane and are referred to as bridging oxygen (BO) and terminal oxygen (TO) sites, respectively. These two oxygen rows are expected when the rutile surface is in contact with aqueous solution, as they allow all titanium atoms in the surface plane to be 6-fold coordinated as in the bulk rutile crystal structure. Previous studies performed under ultrahigh vacuum conditions confirm that the bridging oxygens are present on polished (110) surfaces, although the terminal oxygens are absent.[12] The MUSIC model[8,23] predicts that these bridging oxygens will be either unprotonated or singly protonated in aqueous solutions at pH values of 0−14, and we will use the designations BO and BOH for the unprotonated and protonated bridging oxygens. The MUSIC model also

(7) Westall, J. C.; Hohl, H. *Adv. Colloid Interface Sci.* **1980**, *12*, 265.
(8) Hiemstra, T.; Van Riemsdijk, W. H.; Bolt, G. H. *J. Colloid Interface Sci.* **1989**, *133*, 91−104.
(9) Machesky, M. L.; Wesolowski, D. J.; Palmer, D. A.; Ridley, M. K. *J. Colloid Interface Sci.* **2001**, *239*, 314.
(10) Pauling, L. *J. Am. Chem. Soc.* **1929**, *69*, 542−554.
(11) Brown, I. D. *The Chemical Bond in Inorganic Chemistry−The Bond Valence Model*; Oxford University Press: Oxford, U.K., 2002.
(12) Charlton, G.; et al. *Phys. Rev. Lett.* **1997**, *78*, 495−498.
(13) Griffiths, D. M.; Rochester, C. H. *J. Chem. Soc., Faraday Trans. 1* **1977**, *73*, 1510−29.
(14) Jackson, P.; Parfitt, G. D. *Trans. Faraday Soc.* **1971**, *67*, 2469−83.
(15) Henderson, M. A. *Surf. Sci. Rep.* **2002**, *46*, 1.
(16) Diebold, U. *Surf. Sci. Rep.* **2003**, *48*, 53−229.
(17) Brown, G. E., Jr.; et al. *Chem. Rev.* **1999**, *99*, 77.
(18) Towle, S. N.; Brown, G. E., Jr.; Parks, G. A. *J. Colloid Interface Sci.* **1999**, *217*, 299.
(19) Hayes, K. F.; Katz, L. E. In *Physics and Chemistry of Mineral Surfaces*; Brady, P. V., Ed.; CRC Press: Boca Raton, FL, 1996; pp 147−224.
(20) For a review of XR applied to the mineral−water interface, see: Fenter, P. In *Applications of Synchrotron Radiation in Low-Temperature Geochemistry and Environmental Science*; Fenter, P. A., Rivers, M. L., Sturchio, N. C., Sutton, S. R., Eds.; Reviews in Mineralogy and Geochemistry; Geochemical Society: St. Louis, MO, 2002; pp 149−220.
(21) For a review of the X-ray standing wave technique, see: Bedzyk, M. J.; Cheng, L. In *Applications of Synchrotron Radiation in Low-Temperature Geochemistry and Environmental Science*; Fenter, P. A., Rivers, M. L., Sturchio, N. C., Sutton, S. R., Eds.; Reviews in Mineralogy and Geochemistry; Geochemical Society: St. Louis, MO, 2002; pp 221−266.
(22) Rustad, J. R. In *Molecular Modeling Theory: Applications in the Geosciences*; Cygan, R. T., Kubicki, J. D., Eds.; Reviews in Mineralogy and Geochemistry; Mineralogical Society of America: Washington, DC, 2001; Vol. 42, pp 169−197.
(23) Hiemstra, T.; van Riemsdijk, W. H. *J. Colloid Interface Sci.* **1996**, *179*, 488.

predicts that the three-coordinated oxygens in the Ti−O surface plane do not protonate in the 0−14 pH range. The clean (110) surface in a vacuum also exposes five-coordinated Ti atoms.[12] In the presence of any significant water vapor pressure, these bare Ti atoms immediately chemisorb an oxygen ligand, which in the 0−14 pH range may take the form of a bonded hydroxyl group, which we will designate as TOH, or a doubly protonated oxygen, which we will designate as TOH_2. Whether or not the TOH_2 site represents a "free" water molecule that is chemisorbed to a surface Ti atom, or a "protonated hydroxyl group" formally bonded to a surface Ti atom will be discussed in more detail below. Previous authors have referred to the (110) surface in the presence of very low water partial pressures as "nonhydroxylated" or "associative" if the surface is populated solely by unprotonated BOs and chemisorbed water molecules in the terminal sites, and "hydroxylated" or "dissociative", if the water molecules in the terminal sites dissociate with transfer of a proton to the bridging oxygens, to form BOH and TOH surface species.[24,25]

Assuming no displacements of these surface oxygens from their equivalents in the bulk crystal, the bridging and terminal oxygens would have heights of 1.265 and 1.983 Å with respect to the surface Ti−O plane (Figure 1B). However, prior to the current study, the exact termination and structure of rutile surface in contact with dense liquid water had not been determined experimentally, including any surface structural relaxations. Moreover, little was known about the specific locations of ions adsorbed to this surface, with the exception of the powder and single-crystal extended X-ray absorption fine structure (EXAFS) studies of Brown and co-workers (e.g., refs 18, 26, and 27) and our preliminary X-ray standing wave (XSW) investigations of this surface.[28]

A number of new insights can be obtained through the coordinated multipronged approach employed in this study: (1) Direct experimental observations by X-ray based techniques reveal the key structural features of the rutile surface structure and the locations of adsorbed ions. (2) Comparison of the X-ray results to ab initio calculations and molecular dynamics simulations directly tests our conceptual understanding of these systems and the validity of these models. (3) The sensitivity of the simulations to the proton distributions between the different surface oxygen sites leads to a new understanding of proton site distributions that are not experimentally observable. (4) Integration of these results with surface complexation models tests the ability of SCMs to incorporate precise structural information and leads to more precise and constrained estimates of the parameters that describe ion binding (e.g., binding constants, capacitance values). While this integrated approach does not resolve all questions or ambiguities surrounding ion adsorption by rutile, it does yield new insights into the specific binding sites and hydration states of adsorbed protons and other ions as well as interfacial solvent properties (structure, diffusivity, dielectric constant), all of which are aiding the development of SCMs that can incorporate this atomistic information as fully as possible.

2. Methods and Materials

2.1. Sample Preparation. Polished rutile (110) single crystals (1 cm × 1 cm × 1 mm) used for the X-ray studies were obtained from Princeton Scientific with a typical miscut of 0.1−0.2° with respect to the (110) crystallographic plane. In our earlier study[28] these crystals were used as received, after ultrasonic cleaning in HPLC grade methanol and deionized (DI) water. However, subsequent atomic force microscopy examination revealed a significant amount of surface roughness and/or contamination. The crystal surface topography was greatly improved by the following pretreatment procedure: (a) ultrasonic cleaning in, successively, DI water, 1% HNO_3, high-purity methanol, DI water, 10% H_2O_2 and again, DI water; (b) annealing of the vacuum-dried crystals at 1100 °C for 1 h in an air furnace; (c) hydrothermal reaction in DI water in a Teflon cup housed within a pressure vessel at 220 °C for 12 h; and (d) a final ultrasonic treatment in DI water. This procedure led to the development of apparently atomically flat terraces separated by single unit cell high steps. This improvement in surface quality resulted in superior X-ray data that, while similar, are quantitatively different from previous studies.[28] We believe that the present results are intrinsic to the rutile (110)−aqueous interface.

Surface titration measurements were performed with rutile powders obtained from Tioxide Corp. (14−16 m^2/g) after thorough rinsing and hydrothermal pretreatment[29] and were shown to consist of lathlike, submicrometer crystals exhibiting predominantly (>70%) the (110) crystal face.[30]

2.2. X-ray Reflectivity (XR) Measurements. XR data were measured with photon energy of 14.8 keV at Advanced Photon Source (APS) beamline 1-BM (with preliminary data obtained at beamlines 12-ID-D and 11-ID-D) in a thin-film cell geometry.[20] Reflected intensities were integrated and background subtracted by using ω-scans. The derived reflected intensities, normalized for resolution, active area, Lorentz factor, and incident beam flux, are proportional to $B \cdot T \cdot |F|^2$, where F is the complex structure factor of the rutile−water interface, and B and T account for surface roughness and X-ray beam transmission through the thin water layer, respectively.[20] Crystal truncation rod (CTR) measurements of the rutile−water interface structure were performed with the substrate in contact with deionized water. Measurements of Rb^+ adsorption to rutile were performed with solutions containing $[Rb^+] = 1\ m$ and adjusted to pH = 12 with RbOH. (*m* is used throughout this paper to indicate aqueous concentration in units of molality, moles of solute per kilogram of water, and $\mu m = 10^{-6}$ molal).

2.3. X-ray Standing Wave (XSW) Measurements. XSW experiments were performed at APS beamline 12-ID-D and National Synchrotron Light Source beamline X-15A by simultaneously measuring the Bragg reflected intensity and the element-specific characteristic X-ray Kα fluorescence of the selected ions. Incident photon energies were selected to optimize fluorescent signals, with $E = 17.0$, 17.5, 10.92, and 17.96 keV for Rb^+, Sr^{2+}, Zn^{2+}, and Y^{3+}, respectively. XSW data with the (110), (111), (200), (101), and (211) reflections were measured by using suitably detuned post-monochromator channel-cut Si crystals to collimate and match the incident beam dispersion to the selected Bragg reflections. X-ray fluorescence spectra were collected with a germanium solid-state detector and corrected for dead-time. Solution conditions for the XSW triangulation measurements are 10.49 μm $ZnTr_2$ (Tr^- = trifluoromethanesulfonate, a synthetic, noncomplexing, monovalent anion) at pH = 8.0 (with 156.2 μm HTr, and buffered by the addition of tris(hydroxymethyl)-aminomethane (Tris)), 104.4 μm $SrCl_2$ at pH = 10.7 (with 530 μm NaOH), and 11.2 μm $Y(NO_3)_3$ at pH = 6.11 (88 μm HTr with pH adjusted by addition of Tris).

2.4. Ab Initio Calculations. Periodic density functional theory (DFT) calculations were used to complement the surface adsorption studies in three ways. First, atomic structure calculations of the proposed surface complexes were conducted to test if the hypothesized models would be stable configurations. Second, force field parameters have been developed for TiO_2−

(24) Lindan, P. J. D.; Harrison, N. M.; Holender, J. M.; Gillan, M. J. *Chem. Phys. Lett.* **1996**, *261*, 246−252.
(25) Lindan, P. J. D.; Harrison, N. M.; Gillan, M. J. *Phys. Rev. Lett.* **1998**, *80*, 762−765.
(26) O'Day, P. A.; Chisholm-Brause, C. J.; Towle, S. N.; Parks, G. A.; Brown, G. E., Jr. *Geochim. Cosmochim. Acta* **1996**, *60*, 2515−2532.
(27) Brown, G. E.; Parks, G. A. *Int. Geol. Rev.* **2001**, *43*, 963−1073.
(28) Fenter, P.; et al. *J. Colloid Interface Sci.* **2000**, *225*, 154−165.
(29) Machesky, M. L.; Wesolowski, D. J.; Palmer, D. A.; Ichiro-Hayashi, K. *J. Colloid Interface Sci.* **1998**, *200*, 298−309.
(30) Ridley, M. K.; Machesky, M. L.; Palmer, D. A.; Wesolowski, D. J. *Colloids Surf., A* **2002**, *204*, 295.

H_2O interactions[31] that were used in the molecular dynamics (MD) simulations of this research effort.[32,33] Third, the calculated Ti−O bond lengths in surface BO, BOH, TOH, and TOH_2 groups as well as the H-bonding at the TiO_2-H_2O interface can be used to supplement the calculation of surface oxygen proton affinities using the MUSIC model.[34,35]

A three Ti-layer cell consisting of a 2 × 1 surface rutile unit mesh was created to model adsorption of Sr^{2+} and Zn^{2+} on the (110) surface. This cell consists of two (110) surface unit meshes in the [001] direction and one surface unit mesh in the [1$\bar{1}$0] direction having dimensions of 2.959 and 6.497 Å, respectively. The (110) faces were separated by a vacuum gap of about 15 Å (corresponding to a third translation vector of 24 Å). The atomic positions in the central Ti−O layer were fixed at the experimental bulk crystal geometry to mimic the constraint of the bulk crystal structure. All other atoms were allowed to relax, but the unit cell parameters were constrained to the experimental values. The slab was symmetric (space group *P*-1) about this central plane, and the adsorbed ions were placed on both sides of the symmetric slab. Using this symmetry relation makes the calculations more computationally efficient. For each ion, the adsorbed species was initially placed in a position suggested by the interpretations of the XSW data.

In calculations for Sr^{2+}, three H_2O molecules on each slab side were included on the surface. All of them were initially bonded to the Sr^{2+}. The other five coordination sites were occupied by surface oxygens because Sr^{2+} may have six or eight oxygen atoms in its solvation shell.[36] For calculations with Zn^{2+}, five H_2O molecules were included on each surface, all of them were initially bonded to monodentate Zn^{2+} ($Zn^{2+}\cdot5(H_2O)$) and four to bidentate Zn^{2+} ($Zn^{2+}\cdot4(H_2O)$) because Zn^{2+} is six-coordinate in aqueous solutions.[36]

The minimum energy structures of the slab models were determined using the CASTEP module[37] of Cerius[2] (Accelrys Inc., San Diego, CA). The generalized gradient approximation (GGA) of Perdew and Wang[38] and ultrasoft pseudopotentials were used, allowing us to apply a relatively small plane wave cutoff energy of 340 eV. The default CASTEP Monkhorst−Pack scheme[39] was used for choosing *k*-points. The energy minimization tolerances were 2×10^{-5} eV/atom for the energy, 5×10^{-2} eV/atom for the root-mean squared force, and 1×10^{-3} Å for the root-mean squared displacement.

2.5 Molecular Dynamics Simulations. Molecular dynamics (MD) simulations of the rutile (110)−solution interface[32,33] consist of vacuum-separated sandwiches of 2000 water molecules and dozens of dissolved ions between four-layer TiO_2 slabs, assembled by lateral replication (6 × 12 unit cells) of an ab initio optimized rutile surface unit cell. For studies of the vacuum-terminated surface in contact with dense water, we simulate the two extremes of associative or dissociative water adsorption identified by previous spectroscopic[15] and ab initio[40,41] studies. These include surfaces populated entirely by (a) unprotonated bridging oxygens (BO) in addition to the surface plane containing 3-fold surface oxygens and bare 5-fold surface Ti atoms, designated the "neutral, nonhydroxylated" surface, and (b) protonated bridging oxygens (BOH) and bonded terminal hydroxyls (TOH) in addition to the 3-fold surface oxygens, which is designated the "neutral hydroxylated" surface. The ab initio derived bending potential for Ti−O−H angles was applied; the oxygen and hydrogen atoms in the BO, BOH, and TOH were flexible with fixed bond lengths obtained by ab initio calculations.[31] All other surface atoms were kept rigid.

The SPC/E water model[42,43] is used to simulate liquid water and its interactions with all ions except Zn^{2+}, for which parameters optimized for the simple point charge (SPC) model[44] were used.[33] The SPC/E model does not allow water molecules to dissociate or even polarize, but this model is known to accurately reproduce the physical (phase envelope, dielectric constant, density, viscosity) and structural (hydrogen bonding, ion hydration) properties of real water over wide ranges of temperature, pressure, and electrolyte concentration. Simulations invariably demonstrate that all terminal sites at the neutral, nonhydroxylated surface are immediately occupied by chemisorbed water molecules with near-zero diffusivities. Therefore, the neutral, nonhydroxylated surface is effectively populated by BO and TOH_2 surface sites. Simulations of negatively charged surfaces are obtained by explicitly replacing some chemisorbed water molecules (TOH_2) at the neutral, nonhydroxylated surface with bonded terminal hydroxyl (TOH) groups to form the "charged, nonhydroxylated" surface. Thus, this surface is populated by BO, TOH, and TOH_2 sites. The "charged, hydroxylated" surface is simulated by removing protons from BOH sites on the neutral, hydroxylated surface, with no further tuning of simulation parameters, resulting in a surface populated by BO, BOH, and TOH sites. To obtain a surface charge density of -0.2 C/m^2, 25% of these sites (i.e., 36 sites in our cell) are converted from TOH_2 to TOH on the nonhydroxylated surface, or BOH converted to BO on the hydroxylated surface. Electroneutrality is maintained by manipulating the cation/anion ratio in the adjacent solution, having 48 monovalent cations and 12 monovalent anions or 27 divalent cations and 18 monovalent anions. The resulting concentrations of the bulk solutions are about 0.3 and 0.5 *m*, respectively, derived from the concentration of ions not adsorbed to the surface in the simulations. Additional simulations at -0.1 C/m^2 (pH ∼7) and with different numbers of ions verified that the ion adsorption sites are not sensitive to the exact surface charge and ionic concentration. The length of MD simulations was 1−2 ns with a time step of 1.2 fs.

3. Results

3.1. Interfacial Structure by X-ray Reflectivity (XR) and X-ray Standing Waves (XSW). The three-dimensional arrangement of atoms at the interface between rutile (110) single-crystal surfaces and aqueous electrolyte solutions at 1 atm and 25 °C was determined in situ by using high-resolution XR[20,45] and XSW measurements.[21,46] XR probes the structure at mineral−water interfaces through measurements of weak reflected intensities in the form of crystal truncation rods (CTRs) between bulk Bragg reflections[45] and is the direct analogue of X-ray crystallography for interfacial systems. The reciprocal-space structure of the rutile (110) surface is shown in Figure 2A, showing the crystal truncation rods (as vertical lines) and the rutile Bragg reflections (as filled circles). A surface notation is used to label the truncation rods, and the traditional bulk notation is used for each bulk Bragg reflection (e.g., the (0,2) surface rod intersects the (002), (112), and (222) bulk rutile Bragg reflections, as shown in Figure 2A).

Representative specular and nonspecular XRs for rutile (110) in contact with pure water are shown in Figure 2B. In addition to the (2,0) and (0,2) CTRs that are shown, the (0,0) and (1,1) CTRs were also measured. Together these

(31) Bandura, A. V.; Kubicki, J. D. *J. Phys. Chem. B* **2003**, *107*, 11072−11081.
(32) Předota, M.; Bandura, A. V.; Cummings, P. T.; Kubicki, J. D.; Wesolowski, D. J.; Chialvo, A. A.; Machesky, M. L. Submitted to *J. Phys. Chem. B*.
(33) Předota, M.; Cummings, P. T.; Zhang, Z.; Fenter, P.; Wesolowski, D. J. Submitted to *J. Phys. Chem. B*.
(34) Bandura, A. V.; Sykes, D. G.; Kubicki, J. D. Submitted to *J. Phys. Chem. B* **2003**, *107*, 11072−11081.
(35) Fedkin, M. V.; Zhou, X. Y.; Kubicki, J. D.; Bandura, A. V.; Machesky, M. L.; Wesolowski, D. J. *Langmuir* **2003**, *19*, 3797−3804.
(36) Marcus, Y. *Ion Properties*; Marcel Dekker: New York, 1997; p 259.
(37) *MSI Molecular Simulations User's Guide*: *CASTEP−Cambridge Serial Total Energy Package Version 4.2*; San Diego, CA 1999.
(38) Perdew, J. In *Electronic structure of solids '91*; Ziesche, P., Eschrig, H., Eds.; Akademic Verlag: Berlin, 1991.
(39) Monkhorst, H. J.; Pack, J. D. *Phys. Rev.* **1976**, *13*, 5188.
(40) Zhang, C.; Lindan, P. J. D. *J. Chem. Phys.* **2003**, *118*, 4620.
(41) Langel, W. *Surf. Sci.* **2002**, *496*, 141.
(42) Lee, S. H.; Rasaiah, J. C. *J. Phys. Chem.* **1996**, *100*, 1420.
(43) Palmer, B. J.; Pfund, D. M.; Fulton, J. L. *J. Phys. Chem.* **1996**, *100*, 13393.
(44) Löffler, G.; Schreiber, H.; Steinhauser, O. *J. Chem. Phys.* **1997**, *107*, 3135.
(45) Robinson, I. K.; Tweet, D. J. *Rep. Prog. Phys.* **1992**, *55*, 599.
(46) Zegenhagen, J. *Surf. Sci. Rep.* **1993**, *18*, 199−271.

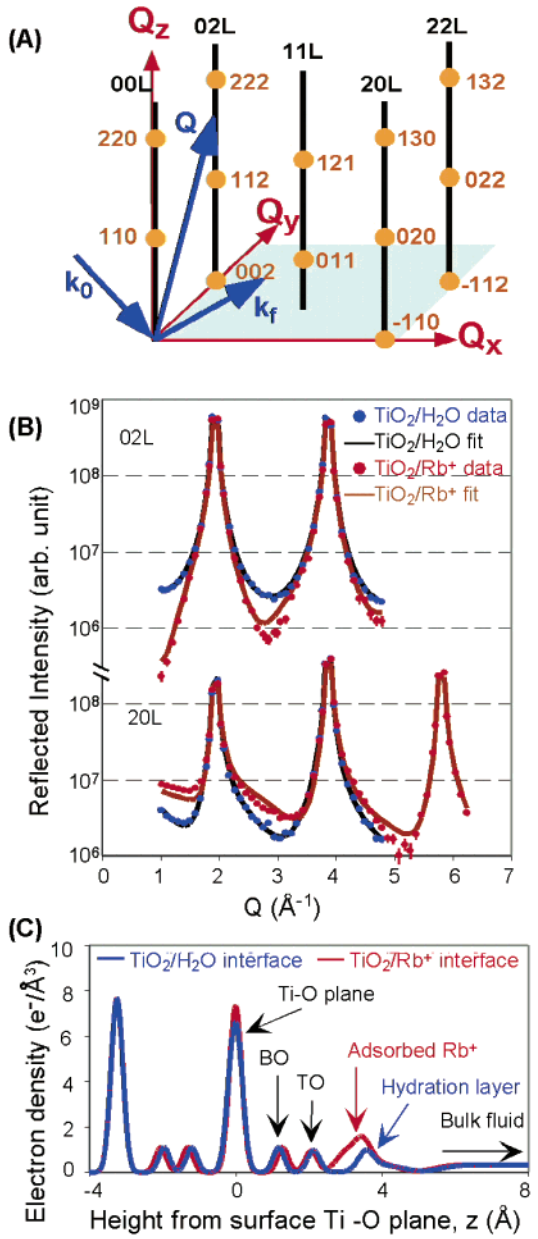

Figure 2. (A) Reciprocal space structure of the rutile (110) surface with crystal truncation rods and bulk Bragg reflections (labeled, with surface Miller indices and bulk Miller indices, respectively). (B) Representative high-resolution XR results for the rutile (110)−water interface, showing the (2,0,L) and (0,2,L) crystal truncation rods for rutile in deionized water (blue circles) and [RbCl] = 1 *m* at pH 12 (red circles), with changes associated with Rb^+ adsorption. Other crystal truncation rods included in this analysis are the (0,0,L), (1,1,L) rods and, in the case of the rutile−water interface data, the (4,0,L) rod. Lines are calculations corresponding to the best-fit structures, whose laterally averaged density profile is shown in (C).

data were quantitatively compared to structural models and optimized to reveal the atomic arrangements at the rutile−water interface. The best fit model was then converted to a laterally averaged electron density profile (taking into account the finite resolution of the experimental data) as shown in Figure 2C. These data reveal that the crystal is terminated by rows of bridging oxygen (BO) and terminal oxygen (TO) sites lying 1.17 ± 0.02 and 2.12 ± 0.02 Å (Figure 2C), respectively, above the surface plane of Ti and O atoms, which are minimally displaced (<0.15 Å) from their locations in the ideally truncated bulk rutile structure (Figure 1). Note, however, that neither XR nor XSW is able to distinguish the protonation state of the surface oxygens. An additional layer of adsorbed water molecules, ~3.8 Å above the surface plane (Figure 2C), is found in laterally ordered sites characterized as bridging between the surface oxygen sites (e.g., BO−TO, TO−TO, and BO−BO sites with 0.92 ± 0.20, 0.69 ± 0.09, and 0.34 ± 0.05 water molecules, respectively, per surface unit cell). This observation is consistent with trends observed in recent studies of hydration layers at other solid−liquid interfaces[47−53] where such ordering appears to be a general phenomenon. Note also that derived oxygen atom locations (as well as sorbed Rb^+ locations discussed below) from these XR data are degenerate to translations of $(a/2)\mathbf{i} + (b/2)\mathbf{j}$ (where a = 6.497 Å and b = 2.959 Å are the surface unit cell dimensions along the [$\bar{1}$10] and [001] directions, respectively) since only a subset of the surface rods, having surface Miller indices $h + k$ = even, were measured. Significantly, no evidence for ordered water is observed beyond this first hydration layer.

XSW measurements reveal element-specific information about interfacial ion distributions[21,46] through a modulation of characteristic fluorescence. This modulation in X-ray fluorescence is due to a shift of the XSW field (red vertical lines, Figure 3A) upon rotating the substrate crystal through its Bragg reflections. Each XSW measurement for a given substrate Bragg reflection, $H = hkl$, can be characterized by two unitless parameters, the coherent fraction, f_H, and coherent position, P_H. As a general definition, these parameters correspond to the amplitude and phase of the H^{th} Fourier component of the fluorescing element distribution. For a single ion location the interpretation is simplified: the coherent position indicates the $\Delta d/d$ ion location with respect to the diffraction planes. ($P = 0$ or 1, corresponds to the ion being on the H^{th} Bragg plane; $P = 0.5$ corresponds to an ion located exactly halfway between the H^{th} Bragg planes.) The coherent fraction describes the ion order. Namely, $f = 1$ if all ions were located at the same $\Delta d/d$ position, and $f = 0$ if the ions form a perfectly random distribution. XSW measurements using the rutile (110) reflection (Figure 3B, Table 1) show that Sr^{2+}, Zn^{2+}, and Y^{3+} specifically adsorb to the rutile surface (pH ~6 to 11 and $[Me^{z+}]_{aq} < 10^{-4}$ *m*) as indicated by the relatively large coherent fractions, f_H. In contrast, no Rb^+ ordering is observed in dilute solutions (pH ~ 11 and $[Rb^+]_{aq} < 10^{-3}$ *m*) as indicated by the small (indistinguishable from zero) coherent fraction for Rb.

To obtain a full three-dimensional location of the adsorbed ions, we performed XSW measurements with the (110), (111), (101), (200), and (211) rutile Bragg reflections. The measured coherent positions, P_H, and fractions, f_H, for these measurements are listed in Table 1. Precise ion locations are determined by XSW triangulation[21,54] (i.e., three-dimensional comparison of noncol-

(47) Fenter, P.; Geissbühler, P.; DiMasi, E.; Srajer, G.; Sorensen, L. B.; Sturchio, N. C. *Geochim. Cosmochim. Acta* **2000**, 1221−1228.
(48) Chu, Y. S.; Lister, T. E.; Cullen, W. G.; You, H.; Nagy, Z. *Phys. Rev. Lett.* **2001**, *86*, 3364.
(49) Reedijk, M. F.; Arsic, J.; Hollander, F. F. A.; de Vries, S. A.; Vlieg, E. *Phys. Rev. Lett.* **2003**, *90*, 066103(1−4).
(50) Eng, P. J.; Trainor, T. P.; Brown, G. E., Jr.; Waychunas, G. A.; Newville, M.; Sutton, S. R.; Rivers, M. L. *Science* **2000**, *288*, 1029−1033.
(51) Cheng, L.; Fenter, P.; Nagy, K. L.; Schlegel, M. L.; Sturchio, N. C. *Phys. Rev. Lett.* **2001**, *87*, 156103(1−4).
(52) Schlegel, M. L.; Nagy, K. L.; Fenter, P.; Sturchio, N. C. *Geochim. Cosmochim. Acta* **2002**, *66*, 3037−3054.
(53) Fenter, P.; McBride, M. T.; Srajer, G.; Sturchio, N. C.; Bosbach, D. *J. Phys. Chem. B* **2001**, *105*, 8112−8119.
(54) Golovchenko, J. A.; Patel, J. R.; Kaplan, D. R.; Cowan, P. L.; Bedzyk, M. J. *Phys. Rev. Lett.* **1982**, *49*, 560−3.

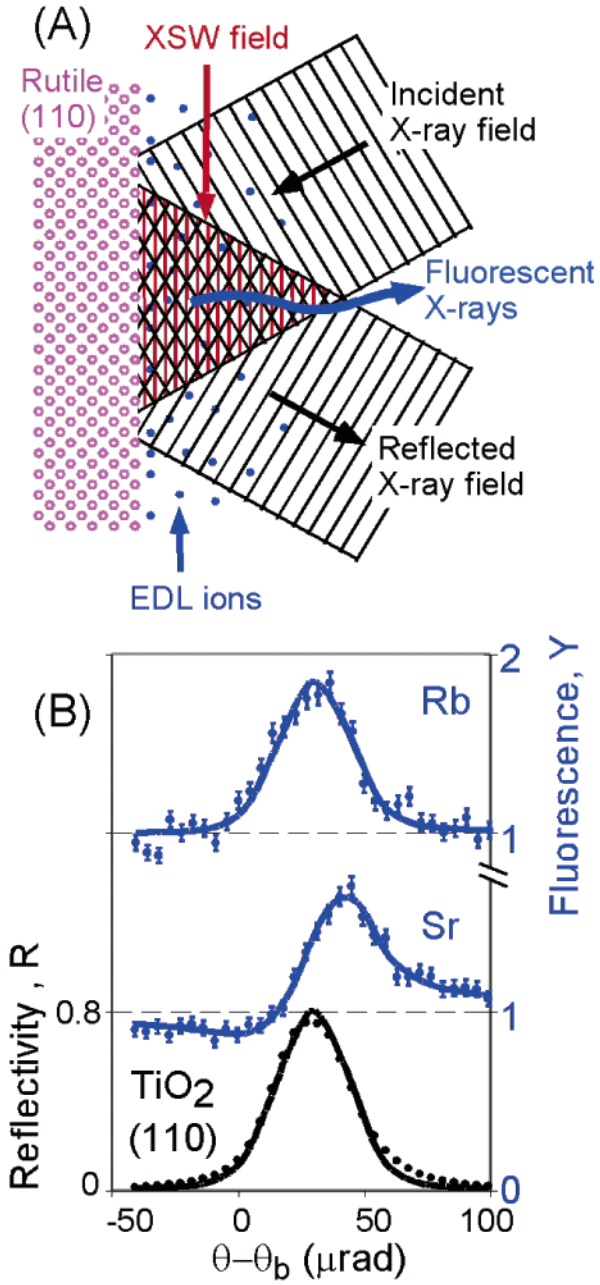

Figure 3. (A) A schematic of the XSW technique showing the incident and Bragg reflected X-ray beams, the EDL ions (that may be either adsorbed to the rutile surface or distributed within a diffuse layer), and the fluorescent X-rays. (B) Representative XSW data for $[Rb^+]_{aq} = 10^{-3}$ *m* at pH = 11.0, and $[Sr^{2+}]_{aq} = 10^{-4}$ *m* at pH = 10.7. The fluorescent yield modulations indicate that Sr^{2+} specifically adsorbs to rutile under these conditions but that Rb^+ does not.

linear XSW results) and by quantitatively comparing measured and calculated values of P_H and f_H for model structures. The calculated results incorporate the multiplicity of ion locations due to the rutile (110) surface symmetry (the two orthogonal mirror planes both perpendicular to the (110) surface), and by averaging over symmetry-equivalent Bragg reflections [e.g., (101), (011), (10$\bar{1}$), and (01$\bar{1}$)]. The starting structures for these comparisons were atom locations obtained from model-independent elemental distributions directly constructed from the XSW data, an approach that was demonstrated recently in the determination of impurities in bulk crystal lattice[55] and atom positions at the vacuum−solid interface.[56] This approach showed that Sr^{2+} and Y^{3+} atoms were located near the "tetradentate site" in which the cation interacts simultaneously with two adjacent BOs and two TOs, while Zn^{2+} was near the atop site above the BO and a bidentate site bridging between TOs.[57] Note that the X-ray based techniques (XSW and XR) are insensitive to the presence of protons at the interface and therefore cannot distinguish between nonprotonated and protonated oxygens. Consequently, for the X-ray results, references to the BO site includes both the BO and BOH species, while the TO site includes the TiOH and $TiOH_2$ species, as defined in the Introduction.

To illustrate the XSW triangulation approach, the derived Sr adsorption structure is shown in side view such that the relevant Bragg planes are perpendicular to the plane of the paper and each structural schematic shows the H^{th} Bragg plane (Figure 4A). If we assume that there is only a single adsorption site, each XSW measurement reveals one component of the ion position with respect to the Bragg diffraction planes along the direction normal to the diffracting plane (defining a plane of allowed locations for each coherent position). In the simplest case the ion position is defined by the intersection of these planes. All of the XSW data can be explained by a single structure in which the Sr^{2+} ion is located near the tetradentate site. There are, however, two distinct tetradentate positions within each rutile (110) surface unit cell that are symmetry-related and therefore equally occupied. For the (110), (200), and (111) diffraction geometries, the two tetradentate sites project onto either the same site or very similar sites. In contrast, the two tetradentate sites project to significantly different positions with respect to the (101) and (211) diffraction planes. In such cases, the coherent fraction is substantially reduced due to the so-called geometrical factor. This geometrical factor reduces the coherent fraction by a multiplicative factor, $\cos(\pi\Delta/d_H)$, where Δ is the separation of the two equally occupied positions along the normal direction of the diffraction plane, and d_H is the *d* spacing of the Bragg reflection.[21] For the (101) and (211) diffraction geometries, the optimal structure has $\Delta/d_H \sim 0.5$, and the coherent fraction for these reflections is close to 0. Consequently adsorption of Sr in the tetradentate site reconciles both the measured coherent positions and fractions.

Full optimization of the Sr^{2+} location was obtained by quantitatively comparing the measured and calculated coherent positions and fractions. In the best-fit structure, the Sr^{2+} ions were observed to be at a height of 3.07 ± 0.07 Å and displaced laterally by $\Delta x = \pm 0.34$ Å and $\Delta y = \pm 0.36$ Å (where *x* is along [1$\bar{1}$0] and *y* is along [001], as indicated in Figure 1) from the ideal tetradentate site (the site laterally equidistant to two BO and two TO sites). Because of the two mirror planes on the rutile surface, there are four possible lateral adsorption positions in each surface unit cell that are not uniquely distinguished with these data. In the calculations we assumed that each of these sites was equally populated with the same height from the surface plane. Note that ion heights derived by XSW are measured relative to the Ti−O plane in the substrate lattice (or equivalently, the ideal position of the (110) surface plane) since the XSW field is generated from deep within with bulk crystal. This is distinct from the actual

(55) Cheng, L.; Fenter, P.; Sturchio, N. C.; Bedzyk, M. J. *Phys. Rev. Lett.* **2003**, *90*, 255503(1−4).
(56) Okasinski, J. S.; Walko, D. A.; Kim, C.-Y.; Bedzyk, M. J. *Phys Rev Lett., Phys. Rev. B* **2004**, *69*, 041401(R).
(57) Zhang, Z.; Fenter, P.; Cheng, L.; Sturchio, N. C.; Bedzyk, M. J.; Machesky, M. L.; Wesolowski, D. J. *Surf. Sci. Lett.* **2004**, *554*, L95−L100.

Table 1. A List of the Measured Coherent Positions, P_H, and Fractions, f_H, that Were Used To Determine the Three-Dimensional Adsorption Sites for Adsorbed Cations through XSW Triangulation To Obtain Precise Ion Sites[a]

		$H = (110)$		$H = (111)$		$H = (200)$		$H = (101)$		$H = (211)$		
		P	f	P	f	P	f	P	f	P	f	χ^2
Zn^{2+}	data	0.95(2)	0.45(3)	0.60(3)	0.31(2)	0.89(4)	0.16(4)	0.91(2)	0.32(2)	0.89(2)	0.38(3)	
(1 pos.)	calcd	0.94	0.44	0.44	0.35	0.94	0.21	0.97	0.30	0.91	0.30	7.67
(2 pos.)	calcd	0.94	0.45	0.52	0.29	0.87	0.15	0.97	0.36	0.90	0.31	5.46
Sr^{2+}	data	0.93(2)	0.53(2)	0.93(3)	0.39(3)	0.53(4)	0.36(6)	0.45(8)	0.09(3)	0.66(5)	0.11(5)	
	calcd	0.95	0.53	0.95	0.38	0.45	0.41	0.47	0.13	0.42	0.13	1.33
Y^{3+}	data	0.83(2)	0.36(3)	0.86(2)	0.50(3)	0.35(3)	0.36(8)			0.34(9)	0.07(5)	
	calcd	0.85	0.43	0.85	0.43	0.35	0.41	0.42	0.06	0.27	0.06	1.79

[a] The last column shows the quality of fit, $\chi^2 = \sum_i\{[(f_H - f_{Hcalc})/\sigma_f]^2 + [(P_H - P_{Hcalc})/\sigma_P]^2\}$, (where, e.g., f_{Hcalc} and σ_f are the calculated coherent fraction and its uncertainty for reflection, H) in comparing the measured and calculated values for the different models. $\chi^2 \sim 1$ corresponds to a fit that is within error of experimental data. The two calculations for the Zn^{2+} data are for a structure with one and two Zn adsorption sites ("1 pos." and "2 pos.", respectively)

location of the surface plane since that has been shown to be slightly displaced from the bulk structural positions from the XR results in Figure 2. This convention will be used throughout this paper, to facilitate direct comparison between the experimental and computational results. It is also important to recognize that the derived lateral displacements are obtained with the assumption that the ion vibrational amplitude is small. Consequently this represents an upper estimate of the actual lateral displacements if the actual vibrational amplitudes are nonzero.

Y^{3+} is found in a position that is similar to that derived for Sr^{2+}, also adsorbing near the "tetradentate" site involving two TOs and two BOs. The height of this ion above the surface plane is 2.75 ± 0.07 Å. Unlike Sr^{2+}, there is little lateral displacement of Y^{3+} away from the ideal tetradentate site (with a net displacement of $\Delta x = -0.15 \pm 0.16$ Å), although the direction and magnitude of this small displacement are consistent with the expectation of a single Y−O bond length to the BOs and TOs.

Similarly, perspective views of the derived location of Zn^{2+} are shown in Figure 4B. The XSW triangulation confirms that the Zn^{2+} ion is predominantly above the BO, ∼3.1 Å above the surface plane (black circle in Figure 4). However, systematic discrepancies between the data and the calculated values of P_H and f_H, imply that this site alone is insufficient to explain the XSW data. (Note, for instance, the discrepancy between the measured coherent position for the (111) reflection and the calculated value that assumes a single monodentate Zn adsorption site.) Inclusion of a second Zn^{2+} adsorption site that bridges between two TO sites as suggested by the model-independent XSW images (gray circle in Figure 4B) improves the agreement substantially. Finally, if we allow the Zn^{2+} ions to displace from the high-symmetry position, we obtain an excellent correspondence between the measured and calculated values. From this we find that the Zn^{2+} ion above the BO is 3.16 ± 0.14 Å above the Ti−O surface plane (with a lateral offset from the BO position, $\Delta x = 0.74 \pm 0.2$ Å, $\Delta y = 0.00 \pm 0.24$ Å) and corresponds to ∼75% of the adsorbed Zn^{2+}. A second minor species is observed between the TO sites 2.70 ± 0.25 Å above the surface plane (with the lateral offset from the high-symmetry site of $\Delta x = 0.0 \pm 0.6$ Å, $\Delta y = 0.00 \pm 0.33$ Å). These results are similar to sorption sites proposed for Co^{2+} on rutile (110) from grazing-incidence EXAFS measurements[18] but provide greater insight and specificity into both the exact location and the distribution between the two sites that cannot be distinguished by EXAFS measurements.

XSW measurements did not reveal any evidence for the specific adsorption of Rb^+ (Figure 3B) at the relatively low Rb^+ ion concentrations ($[Rb^+] < 10^{-3}$ m) necessary for the XSW measurements (i.e., to maintain a small number of Rb^+ ions in the bulk solution with respect to the number of adsorbed ions). However, the Rb Kα fluorescent yield for these and similar data is higher than expected based solely upon its bulk solution concentration, suggesting that Rb^+ ions are associated with the rutile surface (i.e., in a diffuse layer) but not specifically adsorbed to the surface at detectable concentrations under these conditions. XR measurements (Figure 2B) at pH = 12 with $[Rb^+] = 1$ m, however, revealed that some Rb^+ also specifically adsorbs as seen by the significant change in the shape of the CTR when this ion is present at high concentration. The rutile−water interface structure under these conditions is derived from the CTR data shown in Figure 2C along with the (0,0), (1,1), and (4,0) rods (not shown). As in the case of the rutile−water interface, the derived structure is shown as a laterally averaged electron density profile. These data indicate that Rb^+ adsorbs within the surface hydration layer at a height of 3.44 ± 0.03 Å as evidenced by the increase in the electron density. The observation of changes in the nonspecular CTRs directly indicates that the Rb^+ ions are not only adsorbed to the interface but also laterally ordered, with Rb^+ adsorbed at the tetradentate site (Figures 2B and 5). There also appears to be a small shift in the BO and TO heights under these conditions with respect to that found at neutral pH in deionized water (Figure 2C). While this effect appears to be statistically significant as derived from the errors in our data due to counting statistics, we cannot rule out the possibility that this subtle change in the bridging and terminal oxygen heights may be associated with some form of systematic error. Further measurements are in progress to determine the uniqueness of this result as well as the exact location of ordered interfacial water molecules.

Ion and interfacial water locations, derived by XR and XSW, are summarized in Figure 5, showing trends in both the lateral and vertical ion locations. These results provide reasonable adsorbed metal−surface oxygen distances, consistent with the known differences in crystallographic radii for these ions, and are representative of the interfacial ion locations at rutile (110) in neutral to alkaline aqueous solutions over a broad range of solution conditions.

No evidence for specific anion ordering in the EDL was found in these studies. This includes XSW measurements with Br^- as the compensating ion at acidic pH or as ternary complexes with adsorbed cations at alkaline pH. Unlike chlorine, bromine Kα fluorescence can penetrate the water layer so that its location can be directly probed with XSW as described above for the various cations. Furthermore, no significant changes (i.e., ≥0.2 Å) in Sr^{2+} and Zn^{2+} ion heights were observed as a function of ionic strength (as

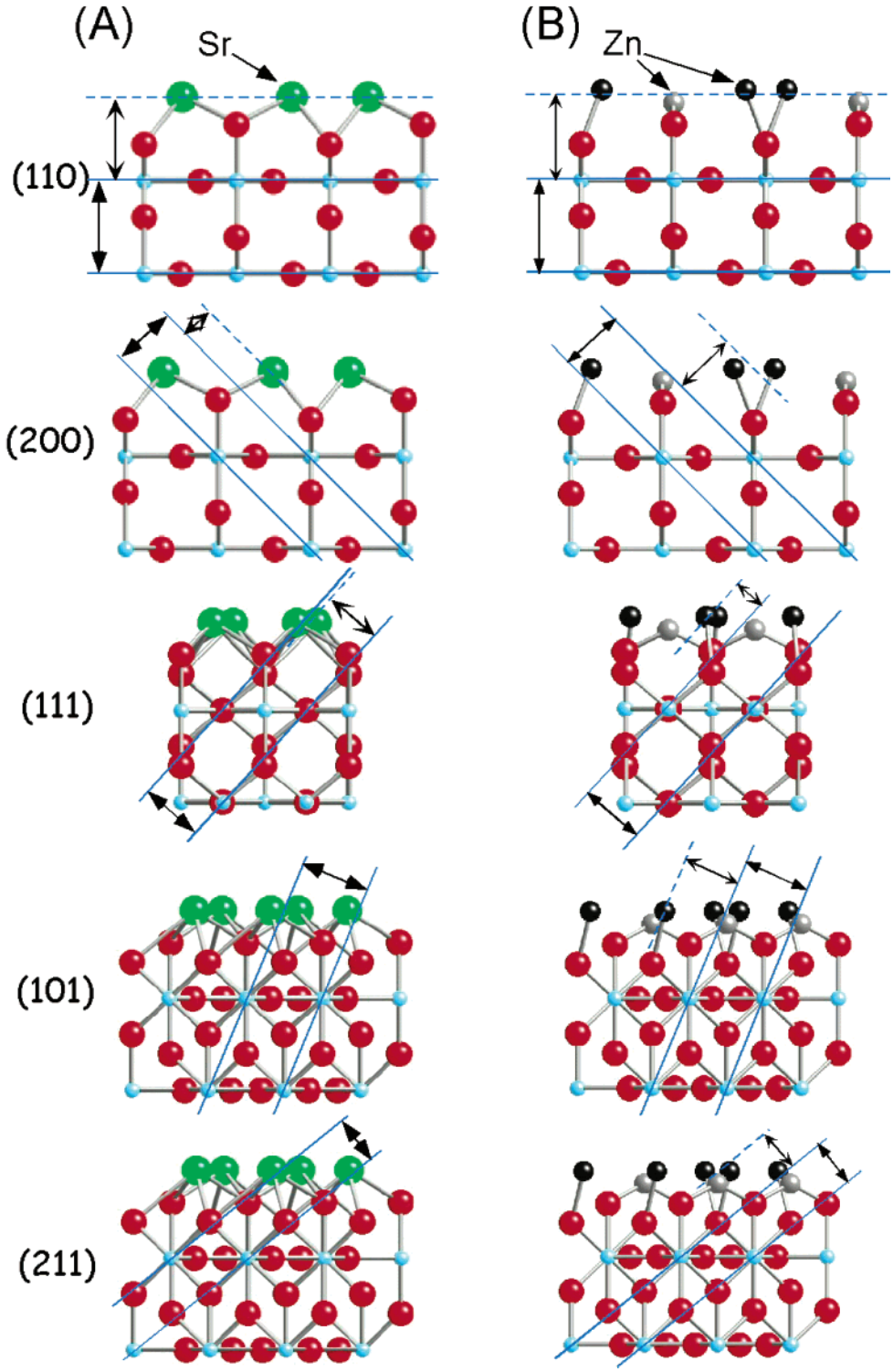

Figure 4. Structural schematics of the derived ion adsorption structures of (A) Sr^{2+} and (B) Zn^{2+}, shown in perspective view so that the diffracting planes are, in each case, perpendicular to the plane of the page (shown as solid lines), and with the nominal ion position indicated by the coherent position shown as a dashed line. Note the large splitting of the Sr atom locations for the (101) and (211) Bragg reflections results in a small coherent fraction, consistent with the experimental data.

high as 1 *m* with NaCl or NaTr as background electrolyte),[58] providing additional indirect evidence that ternary complexes are not formed.

3.2. Ab Initio Calculations. Periodic DFT calculations were used to independently confirm the stabilities of the proposed ion adsorption geometries for Zn^{2+} and Sr^{2+} and provide further insight into the oxygen coordination shell structure of the adsorbed cations, indicating, for instance, that the surface plane oxygen below the tetradentate site is involved in the 8-fold coordination of Sr^{2+}. More generally, the DFT calculations were used to provide a firm foundation for the choice of optimized potentials that were used in the MD simulations to relate the ion and surface proton distributions, complementing the X-ray studies that are insensitive to proton distributions.

(58) Zhang, Z.; et al. In preparation.

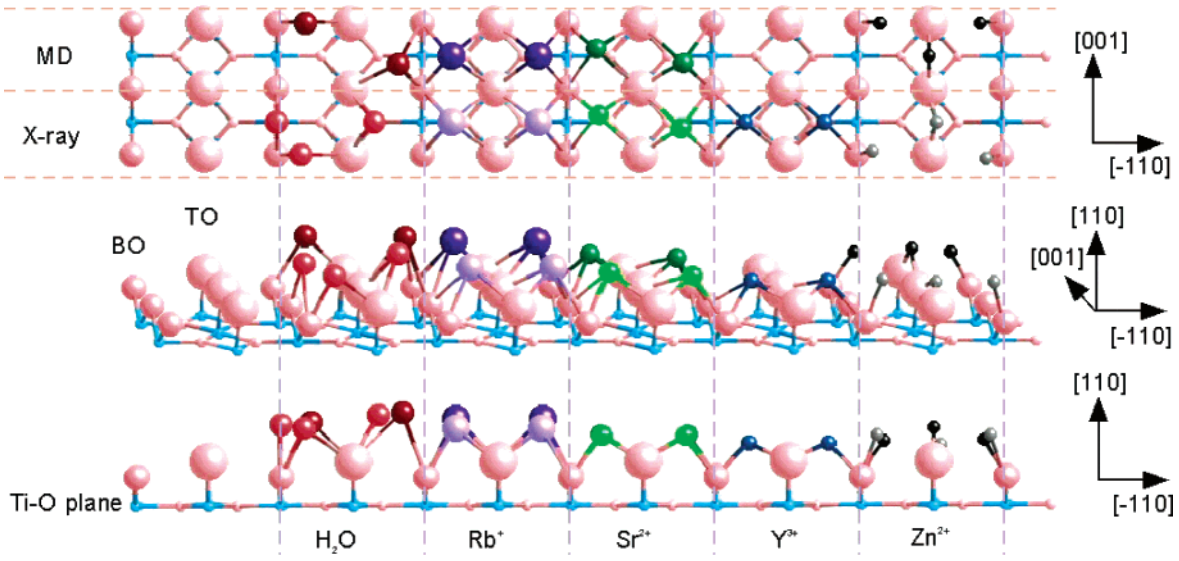

Figure 5. (A) Top, (B) perspective, and (C) side views of the bare rutile (110) surface with bridging and terminal oxygen rows (BO and TO, respectively), and the locations of derived surface hydration and ion adsorption sites, including interfacial water, Rb^{+}, Sr^{2+}, Y^{3+}, and Zn^{2+}. X-ray and MD-derived adatom locations are shaded differently as noted in the top view (the MD results correspond to the hydrated rutile (110) surface). Note the close similarity of ion locations between the X-ray and MD derived ion sites.

Periodic DFT calculations confirm that Sr^{2+} can adsorb in a distorted, 8-fold coordinate environment (Figure 6A). Sr^{2+} is bonded to both the bridging and terminal oxygen atoms in this model, but the Sr^{2+} bond lengths to TOH oxygens are somewhat shorter than the Sr^{2+}−BO bond lengths (2.43 vs 2.66 Å). This difference could be expected because the sum of the Pauling bond strengths to the oxygen atoms in the terminal site is lower than the sum of the Pauling bond strengths to the bridging oxygens. The Sr^{2+} distance from the oxygen atom in the Ti−O surface plane in this calculation is 2.66 Å. The remaining three Sr^{2+}−O(H_2) bond lengths to water molecules above the plane of strongly absorbed ions and water molecules range from 2.72 to 2.82 Å indicating that the ion remains partially hydrated on the surface. All the calculated bond lengths are close to those observed experimentally (i.e., 2.6 Å) for Sr^{2+} in aqueous solutions.[36] The distance from Sr^{2+} to the central plane of the slab is 6.1 Å, resulting in a height above the unrelaxed Ti−O surface plane of 2.85 Å, which can be compared directly with the XSW experimental result of 3.07 ± 0.07 Å.

Monodentate Zn^{2+}·5(H_2O) (Figure 6B) forms a 2.06 Å bond with bridging oxygens on the surface. Five H_2O molecules remain solvating the Zn^{2+} with Zn^{2+}−H_2O bond lengths of 2.01−2.40 Å that are similar to the 2.1 Å distance between Zn^{2+} and H_2O in homogeneous aqueous solution.[36] The separation between the Zn^{2+} ion and the central layer of the slab is 6.66 Å, corresponding to a height above the unrelaxed surface plane of 3.41 Å (compared with 3.16 ± 0.14 Å from XSW measurements).

Bidentate Zn^{2+}·4(H_2O) (Figure 6C) forms two 1.95 Å bonds to the terminal oxygen atoms (TOH). Hence, each bond to the surface is stronger than the monodentate case. The Zn^{2+}−H_2O bond lengths are 1.95 Å for the equatorial bonds and 2.01 Å for the axial bonds. The distance to the central slab is 6.69 Å for this bidentate surface complex, corresponding to a height above the unrelaxed surface plane of 3.44 Å (compared with 2.70 ± 0.25 Å from XSW). This large difference between ab initio and XSW vertical positions for bidentate Zn^{2+} adsorption will be discussed further below.

3.3. Molecular Dynamics Simulations. Molecular dynamics simulations are used to simulate ion distributions while incorporating more experimental details (including the presence of a large number of water molecules and the electrical potential due to surface charge), more thoroughly explore the possible configuration space of ion and water distributions, and provide information about possible ion distributions beyond the first Stern layer. The MD height distributions of oxygen above the Ti−O surface plane reveal peaks near 1.1−1.4 Å for BO sites, and near 2.0−2.2 Å for TOH sites, each shifting further from the surface upon protonation to form BOH and TOH_2 species (Figure 7). The MD simulations confirm the XR observation of an additional layer of sorbed water molecules at ∼3.5−4.0 Å with a distribution that shows discrete lateral sites: bridging the TOH and BO sites and bridging between BO sites (Figure 5). Beyond this strongly sorbed and ordered water layer, the MD simulations indicate only modest layering of water with minimal lateral ordering, in agreement with the XR results.

MD-derived ion axial density profiles of Na^{+}, Rb^{+}, Ca^{2+}, Sr^{2+}, and Zn^{2+} at negatively charged surfaces are shown for nonhydroxylated (Figure 8A) and hydroxylated (Figure 8B) surfaces. Details of the ion vertical and lateral positions are presented elsewhere.[33] Comparison with X-ray results (Figure 5) indicates that the hydroxylated surface is the appropriate description of the charged rutile−water interface with good agreement in the heights (Figure 8B, Table 2) and lateral adsorption sites (Figure 5). For instance, Sr^{2+} exhibits two distinct sorption heights and Rb^{+} has a significant "shoulder peak" on the nonhydroxylated surface (Figure 8A), whereas the X-ray results indicate only one distinct sorption height for these species, as exhibited in the MD simulation of the hydroxylated surface (Figure 8B). On the other hand, Zn^{2+} exhibits only one significant sorption height on the nonhydroxylated surface, versus two distinct heights on the hydroxylated surface, as also seen in the X-ray optimizations, though the absolute values of the two Zn^{2+} sorption heights do not agree. The agreement between X-ray and MD results for Rb^{+} and Sr^{2+} on the hydroxylated surface (Figure 5, 8B) further validates the MD-predicted tetradentate sites for Na^{+} and Ca^{2+} (Figure 8B). MD simulations of the nonhydroxylated surface also show

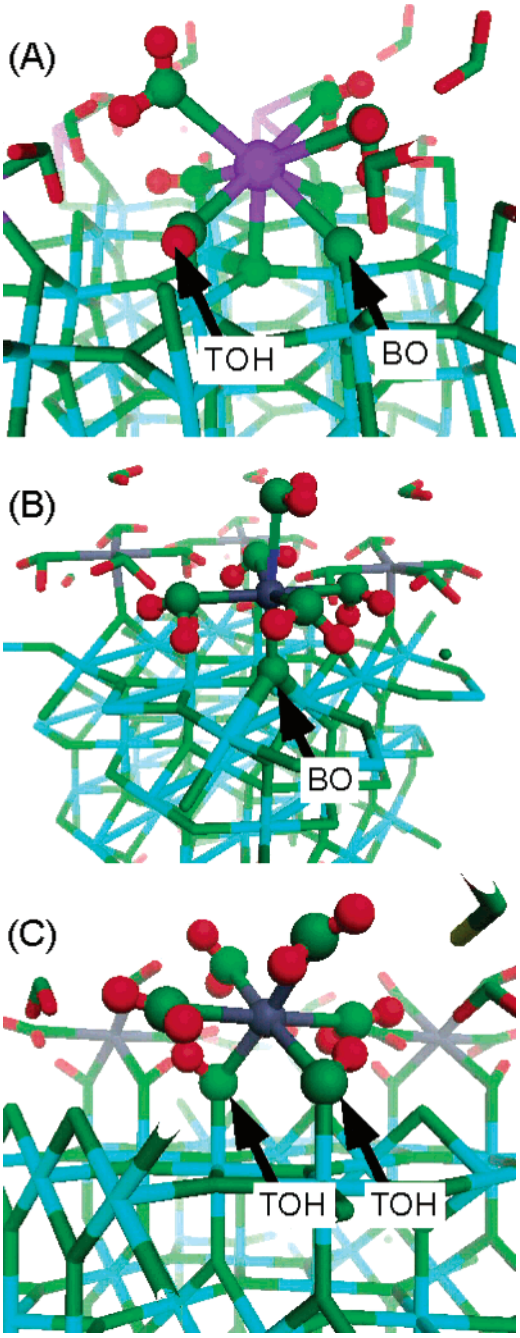

Figure 6. Structures of the calculated ion adsorption structures using ab initio DFT calculations. (A) Sr^{2+} tetradentate is 8-fold coordinate to three H_2O molecules and five O atoms of the TiO_2 surface. (B) Zn^{2+} monodentate is 6-fold coordinate to five H_2O molecules and one bridging O atom of the TiO_2 surface. (C) Zn^{2+} bidentate is 6-fold coordinate to four H_2O molecules and two terminal OH groups. Atoms associated with the surface complex are represented in ball-and-stick mode; all others (including periodic images of the surface complex) are represented using the line mode. H = red, O = green, Ti = teal, Sr = purple, Zn = dark gray.

minor Na^+ and Zn^{2+} ordering at a distance of 5−6 Å above the surface, which would be indicative of "outer sphere" sorption (Figure 8A). These peaks are greatly reduced for the charged, hydroxylated surface (Figure 8B), in agreement with the X-ray results. While the nonhydroxylated (associative) surface may be favored under vacuum conditions,[15] it appears that equilibration of rutile with dense liquid aqueous solutions leads to a surface that is closer to the hydroxylated (dissociative) end-member. The large (∼0.7 Å) difference in Zn^{2+} heights for the bidentate TOH species between the MD hydroxylated surface and the XSW results (Figure 8B) may be due to (a) the accuracy of the X-ray-derived location for this minor (∼25%) species and/or (b) phenomena which cannot be described by the current MD model, such as adsorption of hydrolyzed zinc, $ZnOH^+$, or ion-induced surface changes beyond the flexibility of surface hydroxyls. Another explanation for the discrepancies between modeling (ab initio and MD) and X-ray experiments is that the adsorbed Zn^{2+} ion may undergo a change to 4-fold coordination, but this state has not yet been investigated in the models. Table 2 gives a direct comparison of the sorption heights, relative to the underlying crystal structure, derived from X-ray, ab initio, and MD (hydroxylated surface) results.

Like the X-ray results, the MD simulations do not indicate significant interaction of electrolyte anions with the surface oxygens or sorbed cations. Anions are certainly present in the vicinity of the sorbed cations, but they diffuse rather rapidly and are not ordered. There are several reasons why the adsorption of cations at the rutile (110)−water interface is much more significant than that of anions, such as Cl^-. First, specific adsorption of cations is preferred to anions because the rutile surface is terminated by oxygens, which have an inherent affinity for cations rather than anions. Furthermore, because, the adsorption of Cl^- is weak even at neutral surfaces, anions are repelled by the net surface charge at negatively charged surfaces. Also, whereas the number of adsorbed cations at the surface is about 36 and 18 for the monovalent and divalent cations, respectively, the number of anions at distances smaller than 7.5 Å observed in the simulations is typically only one to two ions. This shows a >10-fold weaker tendency of Cl^- to adsorb at the rutile interface with respect to that of the cations and will be discussed in more detail elsewhere.[33] While no X-ray experimental data on the position of Cl^- at the interface are available, attempts to detect Br^- adsorption by XSW indicated that there was negligible ordering of this anion above the surface, as described above.

A very weak peak of the Cl^- density profile from MD simulation is located at about 5−5.5 Å above the non-hydroxylated surfaces and 6.5 Å for hydroxylated surfaces. Even though the interaction with coadsorbing cations evidently plays a significant role in determining this preferential separation of Cl^- from the surface (in addition to direct interactions with the surface and complex hydrogen structure), the location of these peaks varies by less than 0.3 Å for different cations. The peak density is about 4 times the homogeneous density of Cl^-, as opposed to factor of 20−50 for cations, which demonstrates the low affinity of Cl^- toward the surface. For the neutral hydroxylated surface, an additional small Cl^- peak at 4.3 Å results from direct interaction with hydrogens of surface hydroxyls. In all cases, the lateral distribution of Cl^- is flat, lacking any significant lateral ordering. In terms of site complexation models, this is essentially equivalent to Cl^- being present in the diffuse layer as a truly "indifferent" electrolyte species.

3.4. Integration of Molecular-Scale Structures and Macroscopic Properties. Molecular-scale information can now be used to constrain SCMs that describe proton release and cation adsorption of rutile powders (point of zero net proton charge, $pH_{ppzc} = 5.4 \pm 0.2$ at 25 °C) that predominantly express the (110) crystal face.[30] New powder titration data at 25 °C (Figure 9), using rutile powders similar to those described by ref 30, show features typical of most metal oxide−electrolyte interactions: (1) proton release (Figure 9A) is sensitive to pH and the nature

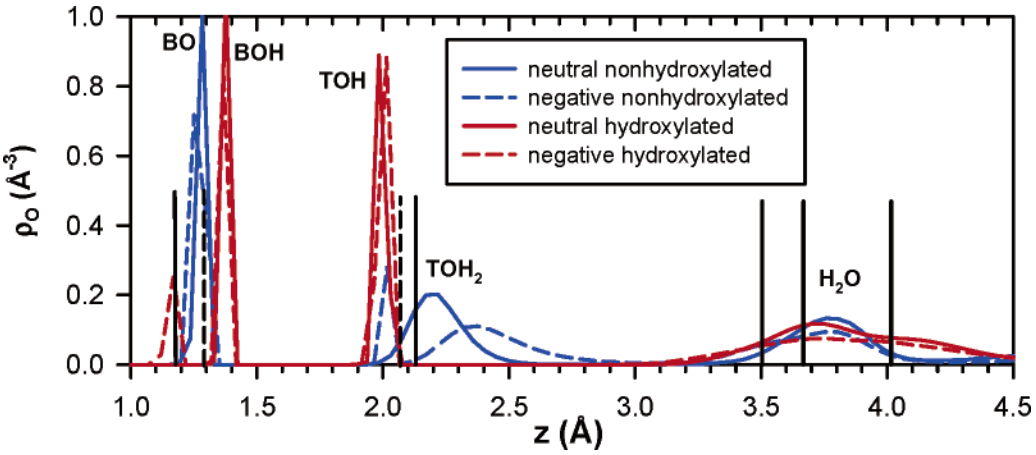

Figure 7. Oxygen density profiles for neutral and charged (−0.2 C/m^2) "nonhydroxylated" and "hydroxylated" surfaces (see main text), including bridging oxygen (BO), protonated bridging oxygen (BOH), hydroxyl group (TOH) and water molecule (TOH_2) in terminal position, and adsorbed water molecules (H_2O), with average oxygen heights obtained from XR shown as vertical lines (dashed vertical lines near BO and TOH indicate locations of these sites at pH 12 upon adsorption of Rb^+).

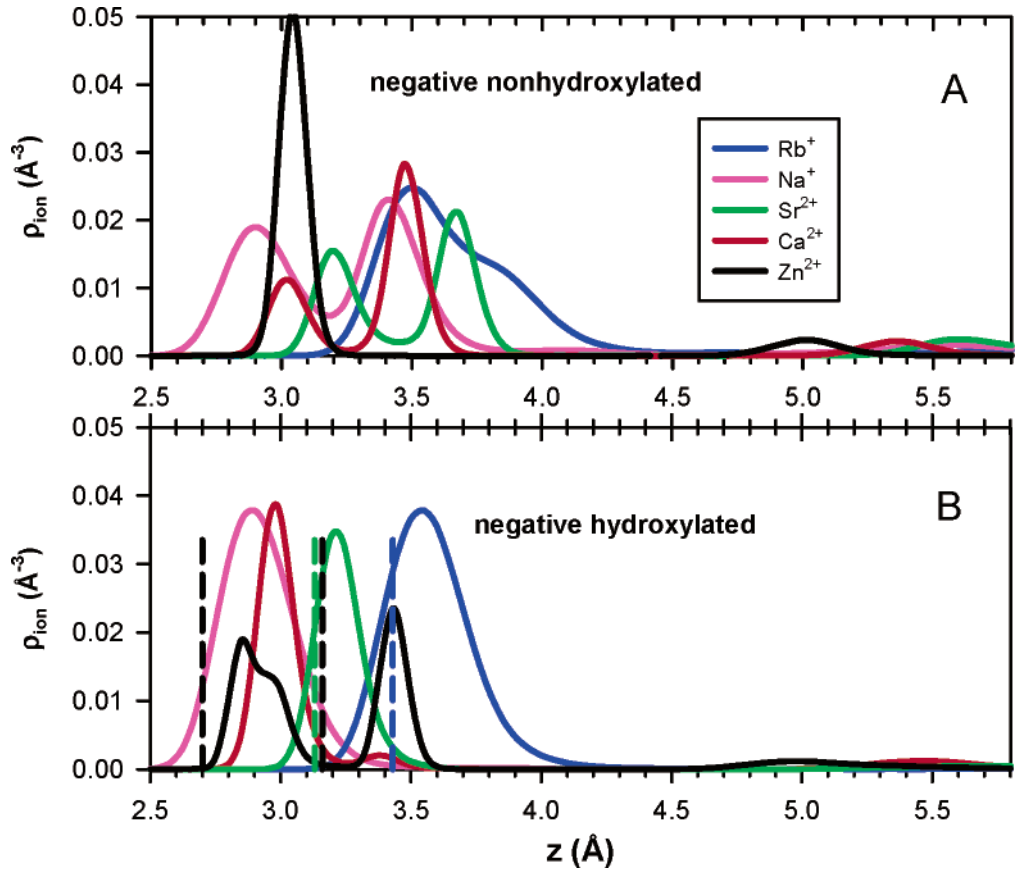

Figure 8. (A) Cation density profiles above the charged, nonhydroxylated surface with surface charge of −0.2 C/m^2. (B) Same as (A), but for the charged, hydroxylated surface, including average ion positions for Rb^+, Sr^{2+}, and Zn^{2+} obtained from XR and XSW, shown as vertical dashed lines color coded according to the legend.

and concentration of an "indifferent" background electrolyte (NaCl, RbCl, NaTr); (2) cation uptake (Figure 9B) isotherms vary strongly with ion type and charge; (3) uptake of weakly bound cations such as Ca^{2+} and Sr^{2+} is significantly influenced (Figure 9B) by the concentration of the "indifferent" background electrolyte (often taken to indicate "outer sphere" adsorption of hydrated ions), while Y^{3+}, Nd^{3+}, Zn^{2+}, and Co^{2+} all show adsorption essentially independent of ionic strength (typically associated with "inner sphere" adsorption).[59]

The revised MUlti-SIte Complexation (MUSIC) model[9,23] allows calculation of proton affinities (K_H) for the BO and TO sites from a Pauling bond valence approach. This treatment indicates that the bridging oxygen is either unprotonated or singly protonated (BO or BOH) in the normal pH range, while the terminal site is a bonded oxygen that is either singly or doubly protonated (TOH or TOH_2). Surface oxygen coordination numbers, Ti−O bond lengths, and the number of donating and accepting H-bonds formed between surface oxygens and associated water molecules are used as inputs to this model. Heretofore, applications of the MUSIC model typically

(59) Hayes, K. F.; et al. *Science* **1987**, *238*, 783.

Table 2. Comparison of Observed and Predicted Heights of Adsorbed Cations above the Unrelaxed Ti−O Surface Plane at the Rutile (110)−Water Interface, Determined with X-ray Reflectivity and X-ray Standing Wave Techniques (X-ray), Ab Initio DFT Calculations, and Molecular Dynamics Simulations (MD) of the Charged, Hydroxylated Surface, Shown in Order of Increasing Crystallographic Ion Radius[a].

ion	ion radii (Å)[c]	ion heights (Å) above unrelaxed Ti−O surface plane[b]		
		X-ray	ab initio	MD
Zn^{2+}	0.75	3.16 ± 0.14 (monodentate)[d]	3.41	2.85, 3.05
		2.7 ± 0.25 (bidentate)[e]	3.44	3.45
Y^{3+}	0.90	2.75 ± 0.07		
Ca^{2+}	1.00			3.0
Na^{+}	1.02			2.9
Sr^{2+}	1.13	3.07 ± 0.07	2.85	3.2
Rb^{+}	1.49	3.44 ± 0.03		3.5
H_2O		∼3.8		3.5−4

[a] Results for the observed water hydration layer are also shown. [b] Indicated by shaded plane in Figure 1A. [c] From ref 36. [d] Majority Zn adsorbed species [e] Minority Zn adsorbed species

assumed the bulk crystal metal−oxygen bond lengths for surface atoms. Also, the revised MUSIC model is ambiguous in that either one or two donating H-bonds are permitted between BO sites and associated water molecules, with the choice arbitrarily resting on the level of agreement between predicted and experimental pH_{zpc} values. Using bulk crystal bond lengths and allowing for two donating H-bonds to the BO sites, Hiemstra et al.[23] estimated the pH_{zpc} at 25 °C for rutile (110) as 5.9, which is close to the average rutile pH_{zpc} value found by Bourikas et al.[60] from their survey of literature values for powdered rutile specimens, but higher than the pH_{zpc} at 25°C for our rutile powder (5.4 ± 0.2).

Our current ab initio calculations indicate relaxed surface bond lengths for the TOH and BO sites of 1.90 and 1.86 Å, respectively. Moreover, MD simulations suggest that the BO site participates in only one H-bond with associated water molecules. With these constraints, the calculated pH_{zpc} for rutile (110) is 5.09 at 25 °C. This is in good agreement with recent second-harmonic-generation studies of the same rutile single-crystal surfaces used in the X-ray studies described above, which indicate a pH_{zpc} for rutile (110) of 4.8 ± 0.2.[61] Increasing both TOH and BO bond lengths by only 0.01 Å, well within the uncertainty of the ab initio results, increases the predicted pH_{zpc} to 5.41, which closely matches our rutile powder value. Although our ab initio and MD simulation results help to constrain our estimated surface protonation constants for rutile, it is important to emphasize how extremely sensitive revised MUSIC model surface protonation constants and resultant estimated pH_{zpc} values are to very small changes in Ti−O bond lengths. Given this sensitivity, and the approximations inherent in our ab initio and MD results to date, the bond length and H-bond constraints will likely be refined in the future. Moreover, the level of agreement with powder titration results will always be influenced by the inherent differences between powders and single-crystal surfaces due to factors such as crystal face distribution and perfection and sample pretreatment procedures. Ultimately, however, ab initio and MD simulations will help in the development of improved MUSIC model approaches to estimating surface protonation constants.

The X-ray and MD results (Table 2) show that on rutile (110) the sorbed cation heights above the surface Ti−O plane scale with bare ionic radii and charge and are insensitive to ionic strength. (Table 2). Figure 10 indicates that, for the tetradentate sorption site, the relationship between ionic radius and adsorbed ion height is approximately linear and independent of cation charge, with Zn^{2+} deviating from this trend due to the fact that it is too small to make contact with all four surface oxygens in this site.[33] Also shown is a calculation of the expected ion height assuming ion close packing with the surface oxygen atoms, ignoring any surface structural displacements. The general agreement (in absolute terms) between the observed and calculated ion heights directly implies that ion heights are primarily controlled by geometrical arrangement of the surface oxygens and the ion size. It must be emphasized that the critical parameter in EDL models is the distance of separation of the sorbed ion centers from the plane of *surface charge*, which in the case of rutile (110) is clearly smaller than the distance of the adsorbed cation centers from the unrelaxed surface Ti−O plane (the shaded plane in Figure 1A), though the two distances are related by a fixed offset. Nevertheless, the relationship shown in Figure 10 directly validates Stern-based descriptions of the EDL which have previously assumed these features. In a strict sense, since each cation resides at a specific height, a full EDL description should include a separate Stern plane for each cation in multicomponent systems. In practice, however, fitting macroscopic ion adsorption data with anything beyond a four-layer Stern model would probably not result in statistically significant improvements in the goodness of fit. Moreover, extensive water structuring is limited to one molecular layer on rutile (Figure 2C), which is inconsistent with a general assumption in the conventional triple-layer model of the EDL in which the capacitance value of the outermost plane is assigned a value of 0.2 F/m^2,[62,63] as argued previously by others.[60,64]

Taken together, the XSW, XR, ab initio, and MD results indicate that all cations are bound as inner-sphere complexes on the rutile (110) surface, consistent with the hypothesis[65] that surface oxygens of oxides with high bulk dielectric constants are able to "hydrate" sorbed cations at least as effectively as solvent molecules. Na^{+} and Rb^{+}, prototypical "indifferent" electrolyte cations, therefore compete directly with Ca^{2+}, Sr^{2+}, and Y^{3+} (and presumably Nd^{3+}) for adsorption at the tetradentate sites. Ionic-strength-dependent uptake of Ca^{2+} and Sr^{2+} on rutile (Figure 9B) is therefore a consequence of relatively weak intrinsic binding of these ions coupled with competition for site occupancy with the more abundant background electrolyte cations, as opposed to the adsorption of the ion as an outer-sphere complex.[59] In the presence of Rb^{+} and Na^{+} alone, however, modeling results indicate that in terms of the total negative surface charge compensation, the diffuse layer contribution always exceeds the Stern layer contribution for all titration conditions reported here (0.03 and 0.3 *m* to pH 10.6).

The powder titration data for Sr^{2+} in RbCl solutions (Figure 9) could be equally well fitted with all possible monodentate, bidentate, and tetradentate bonding configurations (even after incorporating the MUSIC-model-

(60) Bourikas, K.; Hiemstra, T.; Van Riemsdijk, W. H. *Langmuir* **2001**, *17*, 749−756.
(61) Fitts, J.; et al. In preparation.
(62) Davis, J. A.; James, R. O.; Leckie, J. O. *J. Colloid Interface Sci.* **1978**, *63*, 480−499.
(63) Sahai, N.; Sverjensky, D. A. *Geochim. Cosmochim. Acta* **1997**, *61*, 2801−2826.
(64) Hiemstra, T.; Van Riemsdijk, W. H. *Colloids Surf.* **1991**, *59*, 7−25.
(65) Sverjensky, D. A. *Geochim. Cosmochim. Acta* **2001**, *65*, 3643.

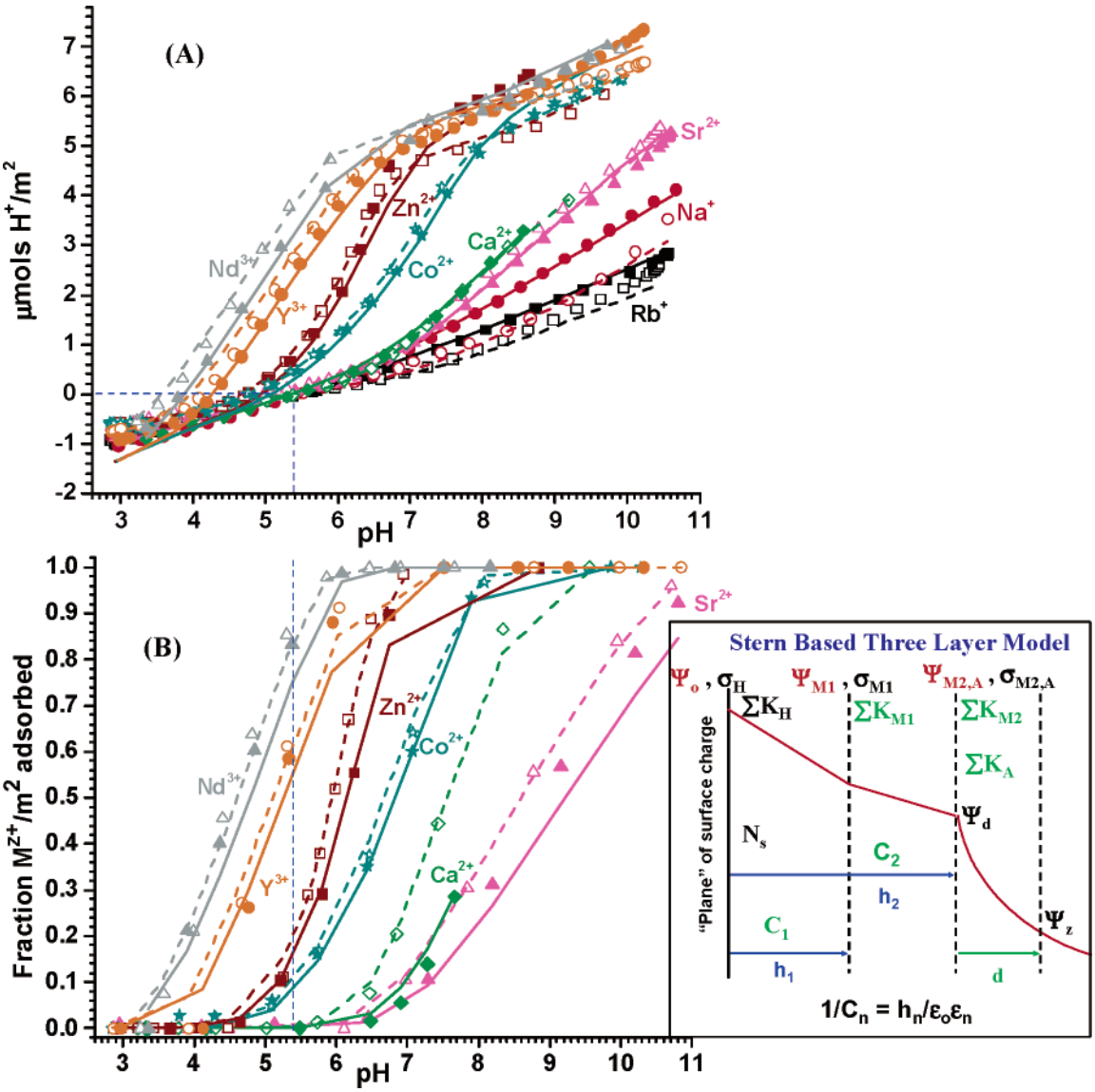

Figure 9. Surface area normalized (m^2) rutile power adsorption data (symbols) and model fits (lines) at 25 °C. Solid symbols and lines = 0.30 *m* background electrolyte (RbCl, NaCl, or NaTr); open symbols and lines = 0.03 *m* background electrolyte. (A) Proton release as a function of solution pH as measured with pH electrodes. (B) Fractional cation adsorption as a function of pH, as measured by the withdrawal and analysis of filtered solution aliquots for the cation of interest. Initial multivalent cation concentrations = 0.001 *m* in all cases. The blue dotted lines identify the pH_{pzc} = 5.4. All data for each cation were fitted simultaneously in generating the model curves, by using explicit formulations of the adsorption structures determined from the present XR and XSW data. Best-fit model parameters are provided in Table 3. The inset in (B) shows the conceptualized EDL model upon which the model fits are based.

calculated K_H values for protonation of BO and TOH sites and the inner-sphere binding of background electrolyte cations using a three-Stern-layer SCM, Figure 9B). The resulting K_{Sr} binding constants and associated capacitance values are similar and reasonable (Table 3). A classical three-layer Stern-based SCM, with the background electrolyte ions sorbing at a single plane and more strongly sorbed multivalent cations sorbing at an additional Stern plane closer to the surface, therefore is generally compatible with our X-ray and MD results. However, this model, without independent atomic-scale ion adsorption data, does not provide unambiguous molecular-level detail regarding reaction stoichiometries and thermodynamic properties.

Because XSW indicates that Sr^{2+} and the dominant monodentate Zn^{2+} surface species are adsorbed at similar heights above the (110) surface plane (Figures 5 and 8B and Table 2), the model-derived capacitance values for the two metals (and by analogy Ca^{2+} and Co^{2+}) should be similar, given that the Stern layer capacitance (C_n) is related to the charge separation distance (h_n, defined in Figure 9B), taken here to be the difference between the cation adsorption height and the average of the BO and TOH heights, ~1.66 Å above the surface plane). However, unreasonably large inner-layer capacitances ($C_1 > 10$) are required to adequately reproduce the powder titration data for Zn^{2+} and Co^{2+} unless additional proton release is included. The titration results can be adequately fit, with C_1 values similar to those for Ca^{2+} and Sr^{2+}, when sorbed Zn^{2+} and Co^{2+} are permitted to hydrolyze, i.e., one or more of the water molecules associated with the sorbed cation releases a proton to bulk solution (Table 4). Moreover, combining the best-fit total Stern layer capacitances for Rb^+ and Na^+ with the heights of these ions obtained from X-ray and MD simulation results leads to a calculated Stern-layer dielectric constant of about 30. This is considerably lower than the bulk water value at 25 °C (78.5), and in such an environment metal ion hydrolysis

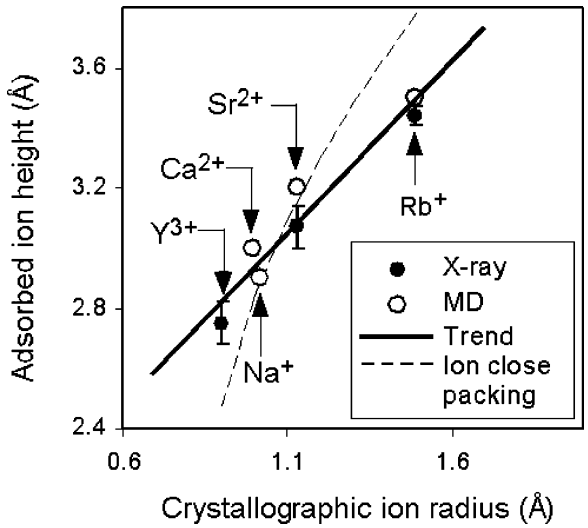

Figure 10. Plot of cation sorption height above the unrelaxed Ti−O surface plane (shaded plane in Figure 1A) versus bare cation radius[36] for cations adsorbed in the tetradentate site on rutile (110). Filled circles are X-ray results; open circles are from MD simulations of the charged, hydroxylated surface (see Table 2). The solid line is a guide to the eye indicating the approximately linear trend relating ion size to ion heights. The dashed line indicates the expected ion height variation assuming it is determined solely by close packing of the bare cation with surface oxygens (with radius of 1.4 Å) at heights of 1.983 and 1.265 Å.

reactions would be enhanced.[66] The first hydrolysis constants (pK_H) of multivalent cations in the bulk solvent are considerably lower for the transition metals ions than for the alkaline earth ions,[67] possibly explaining why surface-enhanced hydrolysis need only be invoked for the transition metal ions. Surface-enhanced hydrolysis of transition metals sorbed to rutile has been suggested previously on the basis of both macroscopic and microscopic data separately (refs 66 and 18, respectively), but this is the first study that quantitatively links both types of input in arriving at this conclusion.

3.5. Anion Interactions. No evidence for specific anion ordering in the EDL was found in these studies, including (a) X-ray measurements with Br^- as the compensating ion at acidic pH (where a positively charged surface would tend to attract anions) or as ternary complexes with adsorbed cations and (b) MD studies with Cl^- as the anion (used to maintain overall charge neutrality). Furthermore, minimal changes (<0.2 Å) in Sr^{2+} and Zn^{2+} ion heights were observed by XSW as a function of ionic strength (as high as 1 *m* with NaCl or NaTr, as background electrolyte), providing additional indirect evidence that metal cation−electrolyte anion ternary complexes are not formed.[58] Consequently, these results do not support the contention that electrolyte anions are frequently involved in the adsorption of divalent metal cations by metal oxide surfaces,[68,69] at least in the case of rutile (110).

All data shown in Figure 9 were obtained for dilute multivalent cations (10^{-3} *m*) in a background electrolyte (NaCl, RbCl, or NaTr at 0.03 or 0.3 *m*), which justifies inclusion of an additional Stern plane (Figure 9B) for adsorption of the background medium. Though this model specifies anion adsorption at the same layer as the background cation, the resulting very small equilibrium constants describing anion adsorption (K_A) indicate minimal adsorption of background electrolyte anions (Cl^-, Tr^-) to at least pH 2.7, providing independent support for the observed absence of specific monovalent anion adsorption from the X-ray and MD results.

4. Discussion and Conclusions

The present study advances our understanding of ion adsorption phenomena at the rutile−water interface in two general respects. First, new results and insights specific to each of the different approaches used in this study (experimental, theoretical, and simulation) were obtained. Second, these results were brought together within the context of a surface complexation model which specifically incorporates the constraints imposed by the atomic-scale details obtained from X-ray and computational approaches, thereby yielding new insight that can only be obtained with this multipronged approach.

The XR and XSW studies revealed the rutile (110)−water interface structure. These data establish (1) the precise termination of the rutile surface with both terminal and bridging oxygen atoms above the Ti−O surface plane, (2) the presence of a single interfacial water layer with water molecules that are both vertically and laterally ordered with respect to the crystallographic structure of the rutile surface, (3) the precise adsorption sites of various ions including Rb^+, Sr^{2+}, Zn^{2+}, and Y^{3+}, showing that all cations adsorb near the tetradentate site, except Zn^{2+} which adsorbs primarily above the BO, but also with a minor contribution that adsorbs between TOH sites, (4) the fact that all cations investigated, including mono-, di-, and trivalent species, form bonds directly with terminal and bridging oxygens, displacing water molecules in the sorbed water layer, (5) the lack of evidence for adsorption of background electrolyte anions or coadsorption with strongly sorbing multivalent cations, and (6) cation adsorption positions and heights that are independent of the solution ionic strength.

The MD simulations were performed with interaction potentials derived from DFT calculations. These MD simulations lead to new insight into the nature of the surface oxygen sites through comparison of predicted ion distributions for hydroxylated (dissociative) and nonhydroxylated (associative) surfaces with the experimental X-ray results, showing that the hydroxylated surface provides a correct description the ion adsorption sites, which is direct evidence that the terminal oxygen sites are appropriately described as chemically bound hydroxyl groups, and not as associated water molecules. This is fully consistent with the application of the MUSIC model to predict the proton affinities of surface oxygens, which provides direct insight into the actual interfacial proton distributions at elevated pH. The excellent overall agreement in derived ion positions further validates the general approach that we adopted of using DFT calculations to define the interaction potentials used in the MD simulations. These results validate the predictions of ion distributions in systems that were not measured experimentally (e.g., Na^+ and Ca^{2+}). No evidence for specific anion adsorption was found over the range of conditions that were studied. This does not imply that anions (as well as monovalent background electrolyte cations) do not populate the diffuse layer at concentrations different from their bulk values but rather that anions appear to be largely excluded from the first layers at which water molecules and partially hydrated cations strongly sorb at

(66) James, R. O.; Healy, T. W. *J. Colloid Interface Sci.* **1972**, *40*, 65.
(67) Baes, C. F., Jr.; Mesmer, R. E. *The Hydrolysis of Cations*; Krieger Publishing Co.: Melbourn, FL, 1986.
(68) Criscenti, L. J.; Sverjensky, D. A. *Am. J. Sci.* **1999**, *299*, 828−899.
(69) Criscenti, L. J.; Sverjensky, D. A. *J. Colloid Interface Sci.* **2002**, *253*, 329−352.

Table 3. Best-Fit Model Parameters for Various Sr^{2+} Adsorption Configurations Are Summarized and Compared with the Tetradentate Configuration That Was Directly Confirmed by XSW, MD Simulation, and ab Initio Calculations[a]

configuration	structure	C_1	SD_{C1}	log K_{Sr}	SD_{KSr}	MSC[b]
tetradentate	$[(Ti{-}OH^{-0.254})_2\ (Ti_2{-}O^{-0.405})_2]\cdots Sr^{2+}$	3.500	0.100	0.200	0.002	5.62
bidentate	$[(Ti{-}OH^{-0.254})_1(Ti_2{-}O^{-0.405})_1]\cdots Sr^{2+}$	3.084	0.074	0.180	0.004	5.78
bidentate	$[(Ti{-}OH^{-0.254})_2]\cdots Sr^{2+}$	2.991	0.070	0.804	0.015	5.78
bidentate	$[(Ti_2{-}O^{-0.405})_2]\cdots Sr^{2+}$	3.550	0.107	0.096	0.002	5.62
monodentate	$[(Ti{-}OH^{-0.254})_1]\cdots Sr^{2+}$	2.918	0.082	0.426	0.133	5.42
monodentate	$[(Ti_2{-}O^{-0.405})_1]\cdots Sr^{2+}$	3.149	0.103	0.071	0.144	5.29

[a] Note that model selection criterion (MSC) values are all similar, signifying a similar degree of goodness of fit, and that the capacitance (C_1) values are all similar and reasonable. The observed tetradentate configuration is therefore not distinguished from the other possible surface complexes. [b] Model selection criterion. Larger value means better goodness of fit.

Table 4. Model Parameters Associated with Surface Complexation Model Fits to the Data in Figure 9[a]

cation, salt	configuration	adsorption complex	C_1	SD_{C1}	C_2	SD_{C2}	log K_{M1}	SD_{KM1}	log K_{M2}	SD_{KM2}	MSC[c]
Rb^+, RbCl	tetradentate	$[(Ti{-}OH^{-0.254})_2\ (Ti_2{-}O^{-0.405})_2]\cdots Rb^+$			1.35	0.08			−1.00	−0.02	5.15
Na^+, NaCl & NaTr[b]	tetradentate	$[(Ti{-}OH^{-0.254})_2\ (Ti_2{-}O^{-0.405})_2]\cdots Na^+$			2.09	0.10			−1.06	−0.02	4.52
Sr^{2+}, RbCl	tetradentate	$[(Ti{-}OH^{-0.254})_2\ (Ti_2{-}O^{-0.405})_2]\cdots Sr^{2+}$	3.50	0.10	1.35		0.20	0.00	−1.00		5.62
Ca^{2+}, NaCl	tetradentate	$[(Ti{-}OH^{-0.254})_2\ (Ti_2{-}O^{-0.405})_2]\cdots Ca^{2+}$	4.24	0.24	2.09		0.40	0.00	−1.06		5.77
Zn^{2+}, NaTr	monodentate	$[Ti_2{-}O^{-0.405}]\cdots Zn^{2+}$	4.24	0.55	2.09		2.60	0.27	−1.06		4.54
	monodentate	$[Ti_2{-}O^{-0.405}]\cdots ZnOH^+$	4.24	0.55	2.09		−3.25	0.32	−1.06		4.54
Co^{2+}, NaTr	monodentate	$[Ti_2{-}O^{-0.405}]\cdots Co^{2+}$	4.24	0.46	2.09		2.30	0.18	−1.06		5.04
	monodentate	$[Ti_2{-}O^{-0.405}]\cdots CoOH^+$	4.24	0.46	2.09		−4.70	0.21	−1.06		5.04
Y^{3+}, NaCl	tetradentate	$[(Ti{-}OH^{-0.254})_2\ (Ti_2{-}O^{-0.405})_2]\cdots Y^{3+}$	6.20	0.33	2.09		6.70	0.04	−1.06		5.71
Nd^{3+}, NaCl	tetradentate	$[(Ti{-}OH^{-0.254})_2\ (Ti_2{-}O^{-0.405})_2]\cdots Nd^{3+}$	6.00	0.60	2.09		8.05	0.08	−1.06		5.10

[a] C_1 is the best-fit inner Stern layer capacitance value (F/m^2), and KM1 the best-fit binding constant for a cation bound at the inner Stern plane. C_2 and KM2 are values for the background electrolyte cation bound at this plane (Rb^+ and Na^+ only). SD refers to 1 standard deviation about a best-fit parameter value, with a blank SD cell signifying that a particular parameter value was held constant. Values for Zn^{2+} and Co^{2+} specify two adsorption complexes that are needed to account for the titration data in Figure 9, including the sorbed, Me^{2+}, and hydrolyzed, $MeOH^+$, species. [b] Sodium trifluoromethanesulfonate. [c] Model selection criterion. Larger means better goodness of fit.

crystallographically dictated sites and that any anions in the diffuse layer are not ordered relative to the crystal surface structure. The exclusion of anions from the surface-contact layer most likely is related to the fact that the surface presented to the solution consists entirely of oxygen atoms, which inherently repel anions.

Titrations using rutile powders dominated by (110) surfaces provide direct measurements of the proton release and specific cation adsorption as a function of pH, in Cl^- and Tr^- solutions of Na^+, Rb^+, Ca^{2+}, Sr^{2+}, Zn^{2+}, Y^{3+}, and Nd^{3+}. The broad pH, ionic strength, and cation charge/radius ranges of these measurements for ions whose adsorption structure was determined by X-ray measurements and MD simulations allow the microscopic structures to be connected to the observed macroscopic manifestations of the EDL structures and properties.

This work points toward a powerful new strategy for compiling experimental and theoretical observations within a single conceptual model, using measured microscopic structural constraints (such as ion height and adsorption geometry) as fixed inputs into the calculation, rather than as fitting parameters. This synergistic approach tests, to a much greater extent than was ever possible before, the ability of the SCMs to properly incorporate this information and provides new insight into EDL properties, which will be critically needed when applying these concepts in rationalizing reaction kinetics at interfaces, such as dissolution, precipitation, adsorption, and heterogeneous catalysis. It was directly shown that various choices for ion adsorption site (even incorrect ones) can be incorporated into SCMs that all adequately fit macroscopic powder titration data and, more importantly, that the exact sorption reaction stoichiometry is ambiguously constrained by applications of SCMs to bulk titration data alone. Thus the SCMs are sensitive to the assumed interfacial geometry but are unable to provide unique, atomic-scale information concerning the interfacial structure. Results of the SCM analysis of Sr^{2+} titration data, exhibiting macroscopic characteristics that are usually associated with outer sphere adsorption (e.g., relatively weak binding and ionic strength dependent uptake curves), are instead explained by adsorption of Sr^{2+} as an inner sphere adsorbate that competes for adsorption with the background electrolyte cation. This latter observation is corroborated by the X-ray reflectivity measurements showing that Rb^+ specifically adsorbs to the same site as Sr^{2+}.

A similar analysis of Zn^{2+} titration data revealed that the proton balance could not be explained by simple ion adsorption but, with the ion height and adsorption site separately defined, proton release was found to be larger than expected for Zn^{2+} and could be explained by surface-enhanced hydrolysis of Zn^{2+}. In comparison of the adsorbed cation positions from the X-ray and MD methods, it therefore may not be surprising that the derived Zn^{2+} positions showed the largest discrepancies between these two approaches. This may reflect the presence of an adsorbed species (e.g., $Zn(OH)^+$) and/or ion coordination geometry (e.g., 4-fold vs 6-fold) that was not included in the MD models. To date, our MD simulations have not been structured to accommodate sorption of a partially hydrolyzed cationic species, and we are just beginning ab initio calculations of the sorption of such species on rutile surfaces. Thus, in this instance, macroscopic powder pH and ion adsorption titrations will guide the further development of molecular level models of the EDL properties.

All X-ray, ab initio, MD, and ion adsorption results are broadly compatible with a Stern-based description of EDL structure. More specifically, for the relatively simple solution compositions we have investigated to date, which consist of trace quantities of a multivalent cation in a background electrolyte, a three-layer, two-Stern-plane representation of the compact region of the EDL (inset, Figure 9B) coupled with a MUSIC model description of surface protonation is consistent with all microscopic and

macroscopic results. For rutile and our solution compositions, these Stern layers are occupied exclusively by partially dehydrated cations bound in inner-sphere fashion, and we find no evidence for the extensive involvement of electrolyte anions in cation binding. Moreover, outer layer capacitance values [as determined by the difference $(1/C_2 - 1/C_1)$ from Table 4] range between 2.2 and 4.1 F/m^2, which are much greater than 0.2 F/m^2 as assumed in the conventional triple layer model description of the EDL. Finally, although our three-layer SCM description is broadly consistent with all microscopic results to date, it is not unique in and by itself, since the macroscopic cation adsorption results are equally well described by other plausible adsorption configurations (Table 3). Consequently, further advances in the development of physically realistic SCMs will depend on incorporating microscopic information from a variety of sources (e.g., spectroscopic, ab initio, MD) to the fullest extent possible.

We have synthesized many aspects of EDL structure and properties for rutile (110), but an important issue remains unresolved. The same SCM (Figure 9B) applied to electrophoretic mobility results for similar rutile powders[35] in 0.001 *m* NaCl solutions indicated a distance (*d*, Figure 9B inset) of >80 Å to the "shear plane", where the zeta potential is conventionally assumed to be established, in good agreement with the calculated EDL "Debye length" (∼100 Å). This appears in marked contrast to the present MD simulations[32] and previous MD and experimental results,[70,71] which indicate that water exhibits a nearly bulklike diffusivity and viscosity as close as 10−15 Å from the surface plane over a wide range of solution ionic strength. The concept of the shear plane as a property of the nonflowing *solvent* thus appears to be misleading; instead it may be a nonequilibrium dynamical property of the *dissolved ions* in the vicinity of a charged surface, although this needs to be confirmed through direct experimental observations and further probing of our MD simulation model.

Acknowledgment. The authors thank the U.S. Department of Energy, Office of Basic Energy Sciences, Division of Chemical Sciences, Geosciences, and Biosciences for support of this research in the project "Nanoscale Complexity at the Oxide-Water Interface". Some of this work was performed at the Advanced Photon Source and National Synchrotron Light Source, which are also supported by the Department of Energy at endstations 12-ID-D, 11-ID-D (BESSRC-CAT, APS), 1-BM (XOR-CAT, APS), and X15A (NSLS). The IEC at NU is supported by NSF and DOE. M.P. acknowledges support by the Grant agency of the Czech Republic (Grant No. 203/03/P083). The constructive comments of a reviewer are gratefully acknowledged.

LA0353834

(70) Mattke, T.; Kecke, H.-J. *J. Colloid Interface Sci.* **1998**, *208*, 562.
(71) Raviv, U.; Klein, J. *Science* **2002**, *297*, 1540−1543.